The macrophage tetraspan MS4A4A enhances Dectin-1-dependent NK cell-mediated resistance to metastasis

Irene Mattiola[1,2,3,4,#], Federica Tomay[1,5,#], Maria De Pizzol[1,5,#,§], Rita Silva-Gomes[1,6], Benedetta Savino[1], Tamara Gulic[1,5,$], Andrea Doni[1], Silvia Lonardi[7], Marie Astrid Boutet[8], Alessandra Nerviani[8], Roberta Carriero[1], Martina Molgora[9,£], Matteo Stravalaci[9], Diego Morone[1,^], Irina Nikolaevna Shalova[10], Yunquin Lee[10], Subhra K Biswas[10], Giovanna Mantovani[11], Marina Sironi[1], Costantino Pitzalis[8], William Vermi[7,12], Barbara Bottazzi[1], Alberto Mantovani[1,8,9,*], Massimo Locati[1,5,*]

[1]Humanitas Clinical and Research Center IRCCS, Rozzano, Italy; [2]Laboratory of Innate Immunity, Department of Microbiology, Infectious Diseases and Immunology, Charité - Universitätsmedizin Berlin, Berlin, Germany; [3]Berlin Institute of Health, Berlin, Germany; [4]Mucosal and Developmental Immunology, Deutsches Rheuma-Forschungszentrum, Berlin, Germany; [5]Department of Medical Biotechnologies and Translational Medicine, University of Milan, Milan, Italy; [6]Graduate Program in Areas of Basic and Applied Biology, Instituto de Ciências Biomédicas Abel Salazar, University of Porto, Portugal; [7]Department of Molecular and Translational Medicine, School of Medicine, University of Brescia, Brescia, Italy; [8]Centre for Experimental Medicine and Rheumatology, William Harvey Research Institute, Barts and The London School of Medicine and Dentistry, Queen Mary University of London, London, UK; [9]Humanitas University, Pieve Emanuele, Italy; [10] Singapore Immunology Network, Agency for Science, Technology & Research (A-STAR), Singapore; [11]Fondazione IRCCS Ca' Granda Ospedale Maggiore Policlinico, Endocrinology Unit, Department of Clinical Sciences and Community Health, University of Milan, Milan, Italy; [12]Department of Pathology and Immunology, Washington University School of Medicine, St Louis, MO, USA.

[§]present address: Dompé Farmaceutici, Milan, Italy

[^]present address: Faculty of Biomedical Sciences, Institute for Research in Biomedicine, Università della Svizzera italiana (USI), Bellinzona, Switzerland

[$]present address: Medical Faculty, Department of Physiology and Immunology, University of Rijeka, Rijeka, Croatia

[£]present address: Department of Pathology and Immunology, Washington University School of Medicine, St Louis, MO, USA

[#]these authors contributed equally to the paper

[*]**Corresponding authors:**

Massimo Locati and Alberto Mantovani

Humanitas Clinical and Research Center, Via Rita Levi Montalcini, I-20090 Pieve Emanuele, Italy.

E-mail: massimo.locati@humanitasresearch.it; alberto.mantovani@humanitasresearch.it

Running title: MS4A4A functional interaction with Dectin-1 in macrophages

ABSTRACT

The plasma membrane tetraspan molecule MS4A4A is selectively expressed by macrophage-lineage cells, but its function is unknown. Here we report that MS4A4A was restricted to murine and human mononuclear phagocytes and was induced during monocyte-to-macrophage differentiation in the presence of interleukin 4 or dexamethasone. Human MS4A4A was coexpressed with M2/M2-like molecules in subsets of normal tissue-resident macrophages, infiltrating macrophages from inflamed synovium, and tumor-associated macrophages. MS4A4A interacted and co-localized with the β-glucan receptor Dectin-1 in lipid rafts. In response to Dectin-1 ligands, MS4A4A-deficient macrophages showed defective signaling and defective production of effector molecules. In experimental models of tumor progression and metastasis, MS4A4A deficiency in macrophages had no impact on primary tumor growth, but was essential for Dectin-1-mediated activation of macrophages and natural killer (NK) cell-mediated metastasis control. Thus, MS4A4A is a tetraspan molecule selectively expressed in macrophages during differentiation and polarization, essential for Dectin-1 dependent activation of NK cell-mediated resistance to metastasis.

Keywords: MS4A4A, tetraspanin, Dectin-1, macrophage, NK cell, tumor biology

INTRODUCTION

Macrophages are central players in the pathophysiology of infections and cancer, being capable of adapting to the local microenvironment assuming a range of different phenotypes. During infections, macrophages sense pathogens through pattern recognition receptors and by the release of immune mediators orchestrate the activation of proinflammatory immune responses. This can be mimicked *in vitro* by the exposure to bacterial compounds and interferon γ (IFN-γ), which promotes a classical activation of macrophages (M1), endowed with pro-inflammatory features. At the opposite side of a spectrum of activation phenotypes, interleukin 4 (IL-4) and other stimuli induce macrophages to acquire an alternative phenotype (M2)[1,2]. Macrophages also coordinate immune responses by complex bidirectional interplay with other immune cells. In tumors, in particular, tumor-associated macrophages (TAMs) establish a network with tumor and host cells supporting a protumoral microenvironment[3,4]. TAMs promote tumor progression by different means, ranging from stimulation of angiogenesis to suppression of adaptive immune responses through the triggering of the activity of inhibitory immune checkpoint molecules, such as PD-L1, PD-L2, and VISTA[5]. Based on this, targeting TAMs represents a major therapeutic option under investigation[3]. Several markers have been reported to identify specific macrophage subsets as well as distinct macrophage activation profiles[6,7,8]. The present study investigated in particular the expression and function of the tetraspan molecule membrane spanning 4-domains A4A (MS4A4A), which belongs to the transcription signature of M2-polarized macrophages and TAMs[6,9]. MS4A4A was selectively expressed in tissue-resident macrophages, in homeostatic as well as in inflammatory conditions, and was highly expressed in TAMs, both in humans and mice. MS4A4A functionally associated with Dectin-1 in macrophage lipid rafts and was required for the full activation of Syk-dependent signaling pathway and consequent production of

cytokines and reactive oxygen intermediates upon Dectin-1 engagement. Though macrophage-selective genetic inactivation of *Ms4a4a* had no impact on primary mesenchymal carcinogenesis and transplanted tumor growth, we found that MS4A4A-deficient macrophages were impaired in their ability to support Dectin-1-dependent cross-talk with natural killer (NK) cells, resulting in uncontrolled metastatic spread.

RESULTS

MS4A4A expression is restricted to macrophages.

Transcriptomic data from others and us have previously identified MS4A4A as a putative marker of human macrophages undergoing IL-4-dependent alternative activation[6,9]. When investigated at the protein level by flow cytometry, macrophages were the only leukocyte population scoring positive, while circulating myeloid (polymorphonuclear neutrophils (PMNs), monocyte subsets, myeloid and plasmacytoid dendritic cells) and lymphoid cells (NK, NKT, T, B) scored negative (Fig. 1a). Monocyte-derived dendritic cells did not express MS4A4A (Supplementary Fig. 1a,b) and were also negative for MS4A6A (Supplementary Fig. 1c,d) and MS4A7 (Supplementary Fig. 1e-f), two other members of the MS4A family highly expressed on macrophages[6]. *In vitro*, MS4A4A expression progressively increased during macrophage colony-stimulating factor (M-CSF)-dependent monocyte differentiation to macrophages (Fig. 1b). When regulation of MS4A4A expression in mature macrophages was investigated, we first confirmed its induction in alternative macrophages activated by IL-4, but not by other stimuli inducing M2-like phenotypes such as transforming growth factor-β (TGF-β) and IL-10 (Fig. 1c). We then identified the glucocorticoid hormone dexamethasone (Dex) as a second potent inducer of MS4A4A expression, alone or in combination with IL-4 (Fig. 1c,d). *MS4A4A* transcript abundance was increased by Dex treatment at 18 h, at which time a significant increase in MS4A4A protein expression was also detected (Fig. 1e,f). Glucocorticoids were also demonstrated to act as potent MS4A4A inducers *in vivo*, as *MS4A4A* transcript levels were strongly upregulated in circulating monocytes isolated from Graves' syndrome patients upon acute exposure to methylprednisolone (Fig. 1g). Conversely, Dex treatment was unable to induce expression of MS4A4A, MS4A6A, or MS4A7 in monocyte-derived dendritic cells (Supplementary Fig. 1). Both in resting macrophages and more prominently

in macrophages activated by Dex and IL-4 in combination, MS4A4A expression was significantly enriched in the $CD163^+$ macrophage subset, while its expression did not correlate with CD36 and CD206 expression (Fig. 1h).

To define MS4A4A expression in tissues, we first interrogated the public gene expression database RefExA, which indicated expression of the *MS4A4A* transcript in several normal human tissues (Supplementary Fig. 2a). Analysis of cell type-specific gene expression revealed that *MS4A4A* expression was restricted to macrophages (Supplementary Fig. 2b). In agreement with those data, immunohistochemical analysis detected MS4A4A expression in several human tissues, including colon, lung, and skin (Fig. 2). Also *in vivo*, combined staining confirmed that MS4A4A expression was restricted to the $CD163^+$ macrophages (Fig. 1b,e,h). Importantly, lung plasmacytoid dendritic cells ($CD303^+$; Fig. 1c), colon dendritic cells ($CD1c^+$; Fig. 1f), and skin Langerhans cells ($CD207^+$; Fig. 1i) did not express MS4A4A. Finally, when MS4A4A expression was investigated in the synovium of early rheumatoid arthritis (RA) patients, a prototypic chronic inflammatory condition, MS4A4A resulted again predominantly expressed by a subset of $CD163^+$ macrophages (Fig. 3a,b) and was not detected in $CD3^+$ T cells, $CD20^+$ B cells, or $CD138^+$ plasma cells (Fig. 3c) infiltrating the inflamed synovium. Taken together, these results indicate that both in normal and in chronic inflammatory conditions MS4A4A expression is restricted to tissue-resident macrophages, where it is upregulated by IL-4 and glucocorticoid hormones.

MS4A4A is not functionally relevant for protumoral functions of tumor-associated macrophages.

The gene expression database TCGA also reported the *MS4A4A* transcript signature in a large number of human tumors (Supplementary Fig. 3a), though in some cases to a lower extent as compared to corresponding normal tissues. Consistent with this,

immunohistochemical analysis detected MS4A4A expression in melanoma, as well as in colon and lung tumors. Combined analysis confirmed that its expression was restricted to $CD163^+$ TAMs (Fig. 4a,c,e), in agreement with results obtained on *in vitro* differentiated human macrophages and in inflamed synovium. A strong correlation between *MS4A4A* and *CD163* transcript levels and, to minor extent, other M2/TAM markers, was also evident in the TCGA cancer dataset (Supplementary Fig. 3b). Importantly, tumor-associated dendritic cells did not express MS4A4A (Fig. 4b,d,f).

As the absence of a specific antibody prevented us from investigating the expression of mouse MS4A4A protein, we evaluated *Ms4a4a* expression at the transcript level by qPCR. Consistent with results obtained in the human setting, macrophages were the only leukocyte population present in mouse spleen with detectable *Ms4a4a* transcripts (Supplementary Fig. 4a). IL-4 or Dex, alone or in combination, strongly augmented *Ms4a4a* expression, while the M1 polarizing treatment IFN-γ and lipopolysaccharide (LPS) failed to induce its expression (Supplementary Fig. 4b). In line with abundant MS4A4A expression detected by immunohistochemistry in human TAMs, we detected elevated levels of the murine *Ms4a4a* transcripts in murine TAMs isolated from animals bearing LCC and B16F1 tumors, as well as xenograft tumors of the human kidney cancer cell line A498 (Fig. 4g).

As *Ms4a4a* was highly expressed in murine TAMs, we investigated its functional relevance for carcinogenesis and tumor progression in different tumoral experimental models. To this purpose, mice with macrophage-selective deletion of *Ms4a4a* were generated. *Ms4a4a* expression was successfully abrogated in bone marrow-derived macrophages (BMDMs) of $Ms4a4a^{fl/fl}Lys^{Cre/+}$ animals (indicated here as $Ms4a4a^{-/-}$; Supplementary Fig. 4c), with no apparent phenotype or impact on the development for any immune cell subset (Supplementary Fig. 4d). When animals were tested, we found no difference in appearance, incidence, and growth of primary tumors in mice having

MS4A4A-competent or -incompetent macrophages, neither in the B16F1 transplanted tumor model (Fig. 4h) nor in a model of mesenchymal carcinogenesis based on 3-methylcholanthrene (3-MCA) exposure (Fig. 4i,j). We conclude that, though highly expressed in TAMs, MS4A4A has no functional relevance for their ability to promote primary tumor growth, at least under the experimental conditions tested.

MS4A4A colocalizes with Dectin-1 in lipid rafts.

In search for a functional role of MS4A4A in macrophages, we considered the structural homology of MS4A proteins with tetraspanins, which are known to engage latero-lateral interactions with other membrane proteins and influence their functional properties[10,11]. By performing a split-ubiquitin yeast two-hybrid screening, an approach previously applied to identify partners of other MS4A members[12], we identified membrane proteins interacting with MS4A4A. These included MS4A4A itself as well as MS4A6A and MS4A7, two other MS4A family members highly expressed in alternative macrophages[6], suggesting that on the macrophage plasma membrane these three MS4A members may interact among themselves. We then validated MS4A4A interaction with itself as well as the other two MS4A proteins in CHO-K1 transfected cells by FLIM-FRET analysis (Fig. 5a–c), which indicates that these proteins likely organize in clusters on plasma membranes. Conversely, FLIM-FRET experiments did not reveal interaction of MS4A4A with the tetraspanins CD63 (Förster radius 1.24 ± 0.15 vs 1.27 ± 0.06 for vector- and MS4A4A-transfected cells, respectively; $p > 0.05$) and CD9 (Förster radius 1.28 ± 0.06 vs 1.26 ± 0.05 for vector- and MS4A4A-transfected cells, respectively; $p > 0.05$). Candidate MS4A4A interactors emerged from the split-ubiquitin yeast two-hybrid screening also included the membrane receptor for β-glucan Dectin-1, whose interaction with MS4A4A also was confirmed by FLIM-FRET analysis (Fig. 5d). Flow cytometry analysis indicated that macrophages had high co-expression of MS4A4A and Dectin-1, both under resting conditions and upon Dex

treatment (Supplementary Fig. 5). Confocal microscopy experiments revealed that MS4A4A and Dectin-1 colocalization was significantly increased by the Dectin-1 agonist zymosan, which also induced a significant increase in the colocalization index of both MS4A4A and Dectin-1 with the lipid rafts tracer CT-B (Fig. 5e-h). Super-resolution stimulated emission depletion (STED) microscopy further confirmed increased colocalization of MS4A4A and Dectin-1 upon zymosan stimulation, as well as increased colocalization of both proteins with CT-B (Fig. 5i-k). Interestingly, treatment with the cholesterol-depleting agent methyl-β-cyclodextrin (MβCD) completely abrogated the zymosan-induced increase in Dectin-1 colocalization with MS4A4A (Fig. 5i-l). Taken together, these results indicate that, upon exposure to Dectin-1 agonists, MS4A4A and Dectin-1 colocalizes in lipid rafts on the macrophage plasma membrane, suggesting a functional relevance of MS4A4A on Dectin-1 signaling.

MS4A4A is required for Dectin-1 signalling activity.

We next investigated the role of MS4A4A in Dectin-1 function. Dectin-1 was similarly expressed on BMDMs generated from *Ms4a4a*$^{-/-}$ and wild-type mice, and no difference was observed in the rate of Dectin-1 internalization induced by its agonist zymosan (Fig. 6a). Similarly, binding of zymosan-FITC particles was identical in BMDMs generated from *Ms4a4a*$^{-/-}$ and wild-type animals (Fig. 6b). MS4A4A expression was also not relevant for Dectin-1 internalization and phagocytosis when *Aspergillus fumigatus* conidia were used (Fig. 6c).

In order to investigate the relevance of MS4A4A for Dectin-1 signaling, phosphorylation events for the three main signaling pathways acting downstream Dectin-1 (Syk, p38, and ERK) were assessed in BMDMs generated from *Ms4a4a*$^{-/-}$ and wild-type mice. Upon zymosan challenge, only Syk phosphorylation was significantly reduced in *Ms4a4a*$^{-/-}$ as compared to wild-type BMDMs (Fig. 6d), while ERK and p38 phosphorylation

was unaffected (Fig. 6e-f). Similar results were obtained when curdlan and depleted zymosan, two Dectin-1-specific agonists, were used, but not when BMDMs were stimulated with phorbol 12-myristate 13-acetate (PMA) (Supplementary Fig. 6a–c). Neither p38 nor ERK phosphorylation were influenced by MS4A4A expression with any of the stimuli used (Supplementary Fig. 6d-e). In accordance with reduced Syk phosphorylation, upon zymosan challenge *Ms4a4a*$^{-/-}$ BMDMs released less pro-inflammatory cytokines, including IL-6 and tumor necrosis factor (TNF), and produced less ROS as compared to wild-type BMDMs (Fig. 6g–i). The same defect was observed when depleted zymosan and curdlan were used (Supplementary Fig. 6f,g,i,j). Of note, the absence of MS4A4A did not impact on cytokine production by BMDMs stimulated with TLR agonists, such as LPS (Fig. 6g–h) or Pam3Cys (Supplementary Fig. 6h,k).

Taken together, these results indicate that MS4A4A is dispensable for Dectin-1-mediated microbial recognition and phagocytosis, but is required to support optimal Syk phosphorylation and production of inflammatory cytokines and ROS following Dectin-1 engagement.

MS4A4A contributes to Dectin-1-mediated protection against metastasis.

Dectin-1 has recently been shown to allow dendritic cell/macrophage-dependent recognition of tumor-associated molecular patterns on some tumor cells[13]. This Dectin-1-mediated recognition pathway was shown to have an impact on the metastatic potential of the low metastatic B16F1 melanoma cells. Conversely, this pathway had no relevance for the metastatic potential of the highly metastatic B16F10 melanoma cells, which were found negative for the appropriate N-glycan structures recognized by Dectin-1[13]. In accordance with this evidence, we observed a higher binding of wheat germ agglutinin (WGA), which recognizes N-acetylglucosamine residues, on the surface of B16F1 cells as compared to B16F10 cells (Fig. 7a). As shown for the pathogen-derived Dectin-1 agonists, the tumor

B16F1 cells were able to trigger Syk phosphorylation and cytokine production by BMDMs. Importantly, both Syk phosphorylation and IL-6 secretion induced by B16F1 cells were reduced in *Ms4a4a*$^{-/-}$ as compared to wild-type cells (Fig. 7b,c).

Prompted by this observation, we assessed the relevance of Dectin-1 and MS4A4A expression in macrophages for the metastatic potential *in vivo* of B16F1 and B16F10 cells. In agreement with earlier observations[13], B16F1 cells showed a significant higher metastatic potential in Dectin-1-deficient animals (*Clec7a*$^{-/-}$) compared to wild-type mice, whereas no difference was observed in the number of metastasis generated by B16F10 cells (Fig. 7d,e, respectively). Similarly to previous observations on Dectin-1-deficient animals[13], macrophage-specific *Ms4a4a* deletion had no effect on the metastatic spreading of B16F10, but resulted in a significant increase in the number of B16F1 metastasis, whose metastatic potential became comparable to that of B16F10 (Fig. 7f,g, and Supplementary Fig. 7a). Of note, the number of B16F1 metastasis was not further increased when mice double-deficient for *MS4A4A* and *Dectin-1* (*Ms4a4a*$^{-/-}$*Clec7a*$^{-/-}$) were used, consistent with the idea the two molecules cooperate in a common recognition pathway (Supplementary Fig. 7b). Importantly, the increased B16F1 metastatic spreading observed in the absence of Dectin-1 or MS4A4A was also evident when N-glycans-depleted B16F1 cells were injected in wild-type animals (Fig. 7h). Similar experiments were then performed with two colon carcinoma cell lines that exhibit different metastatic potential. As observed for B16 cells, the low metastatic MC38 cells showed high WGA binding and an increased number of metastasis when injected in both *Clec7a*$^{-/-}$ and *Ms4a4a*$^{-/-}$ mice as compared to wild-type mice (Supplementary Fig. 8a,b,d). Conversely, the highly metastatic SL4 cells, which showed lower WGA binding as compared to MC38 (Supplementary Fig. 8a), generated the same number of metastasis in both *Clec7a*$^{-/-}$ and *Ms4a4a*$^{-/-}$ animals compared to wild-type animals (Supplementary Fig. 8c,e). Taken together, these results suggest that the expression of MS4A4A on macrophages is

279 required for Dectin-1-mediated control of metastatic spreading of highly N-glycosylated
280 tumor cells.

281 *In vitro* experiments have identified NK cells as effector cells in B16F1 killing[13].
282 Consistent with this, NK cell depletion by the use of an anti-NK1.1 antibody resulted in a
283 significant increase in B16F1 lung metastasis and abrogated the difference observed
284 between *Ms4a4a*$^{-/-}$ and wild-type animals (Fig. 8a,b). Conversely, NK cell depletion did
285 not abrogate the difference observed in the number of MC38 liver metastasis
286 (Supplementary Fig. 8d). As confocal microscopy analysis showed that NK cells and
287 macrophages were located in close proximity in B16F1 lung metastasis, suggesting a
288 possible cross-talk between NK cells and macrophages in metastatic lesions
289 (Supplementary Fig. 7c), we then investigated the role of macrophage MS4A4A in NK cell
290 activation. Though *Ms4a4a* deletion had no impact on the abundance of NK cells and
291 macrophages in the lungs bearing B16F1 metastatic lesions (Fig. 8c for NK cells;
292 Supplementary Fig. 7d-g for macrophages), macrophage expression of MS4A4A was
293 required for optimal recognition by NK cells of tumor targets. NK cell cytotoxicity, assessed
294 *in vitro* as the frequency of CD107a^{+} cells in a degranulation assay, was significantly lower
295 when B16F1 cells were cultured with splenocytes from *Ms4a4a*$^{-/-}$ mice as compared to the
296 wild-type counterpart (Fig. 8d). Of note, defective activation of NK cells was not observed
297 when B16F10 cells were used as targets (Supplementary Fig. 7h).

298 Previous studies suggested that Dectin-1 triggering by tumor cells induces the
299 expression on macrophage plasma membrane of calcium homeostasis modulator family
300 member 6 (CALHM6), also known as IFN regulatory factor 3-dependent NK-activating
301 molecule (INAM), which in turn promotes NK cell activation leading to tumor cell killing[13].
302 Consistent with this, the induction of *Calhm6* expression in BMDMs cocultured with B16F1
303 cells was defective when *Ms4a4a*$^{-/-}$ cells were used (Fig. 8e). A similar defect was
304 observed when Dectin-1 ligands were used, but not when BMDMs were activated using

LPS (Supplementary Fig. 7i,j,k). The lack of MS4A4A also affected the cytokine profile induced in BMDMs by tumor cell recognition. While induction of *Il12p40* after B16F1 engagement did not require MS4A4A expression on BMDMs (Fig. 8f), *Ms4a4a*$^{-/-}$ BMDMs expressed significantly less *Il15* and *Il18* transcripts as compared to wild-type BMDMs (Fig. 8g,h respectively). A similar defect was evident when BMDMs were stimulated with zymosan (Supplementary Fig. 7l). In accordance with this finding, IFN-γ production by NK cells was significant lower when B16F1 cells were cocultured with *Ms4a4a*$^{-/-}$ splenocytes as compared to wild-type littermates (Fig. 8i). Taken together, these results are consistent with a non-redundant role of MS4A4A expression in macrophages in controlling tumor metastatization by supporting a Dectin-1-dependent recognition of N-glycans on tumor cells and triggering NK cell-mediated tumor cell killing.

DISCUSSION

MS4A4A is a member of the MS4A family, encoded in a 600 Kb region on chromosome 11q12-13 in human and chromosome 19 in mouse genome[14,15]. MS4A4A has been reported by us and by others as a macrophage-restricted transcript associated with M2/M2-like polarization, and genome-wide association studies have correlated SNP variants within the MS4A4A/MS4A6A locus with late onset Alzheimer's disease and cutaneous systemic sclerosis[16] Recent studies have described MS4A4A as a chemosensor expressed by necklace sensory neurons[17] and as a partner of the receptor tyrosine kinase KIT in mast cells[18], but its function in macrophages is unknown.

MS4A proteins are characterized by a common structural organization based on four putative highly hydrophobic transmembrane domains, two extracellular loops, and short cytoplasmic N- and C-terminals, tightly resembling tetraspanins[19]. Tetraspanins, a large family of cell-surface proteins with a similar structural organization, are known to establish homo and heterocomplexes called tetraspanin-enriched microdomains in which they engage lateral interactions with different partners, influencing their trafficking and signalling properties[11,20,21,22]. Of note, some MS4A proteins, including CD20/MS4A1, FcεR1β/MS4A2, and the highly MS4A4A-related protein MS4A4B, have been shown to enter oligomeric complexes in lipid rafts, where they interact and influence signalling properties of associated partners[12,23,24]. Furthermore, MS4A4A has been reported to regulate the signalling activity of the receptor tyrosine kinase KIT controlling its endocytic recycling and degradation pathways by a mechanism that involves colocalization of KIT with caveolin-1 in lipid rafts in mast cells[18]. Here we have demonstrated that, after Dectin-1 engagement by zymosan, Dectin-1 and MS4A4A translocate in lipid rafts on macrophage plasma membrane. Of note, Dectin-1 has already been reported to interact with tetraspanins, which control its availability on the plasma membrane and the quantity of

cytokines produced after zymosan engagement[25]. Finally, we also provided evidence of MS4A4A association with itself and with MS4A6A and MS4A7, other two members of the MS4A family with a macrophage-restricted expression pattern, and showed that in the absence of MS4A4A expression the signalling properties of Dectin-1 are affected. Taken together, our results suggested that these three MS4A proteins might contribute to the organization of specific microdomains on the plasma membrane of macrophages where signalling properties of membrane receptors, including Dectin-1, are regulated.

Dectin-1 is a pattern recognition receptor belonging to the non-classical C-type lectin receptor family[26]. Dectin-1 plays a pivotal role in controlling a wide range of fungal infections, including species of *Candida*, *Aspergillus*, *Pneumocystis*, and *Coccidioides*[26,27]. More recently, a role of Dectin-1 in the resistance to a broader range of microorganisms, in autoimmunity, and in tumor cell recognition has also been recognized[28]. The signalling activity of Dectin-1 after ligand engagement requires clustering into a phagocytic synapse[29] and results in enhanced phagocytosis, respiratory burst activity, and inflammatory cytokines secretion[30,31]. The Dectin-1 signalling pathway in macrophages is still ill defined[32,33,34]. It has however been demonstrated that Dectin-1 signaling activity in macrophages is delayed as compared to dendritic cells, and that it leads to both Syk-independent and Syk-dependent signalling pathways, which control phagocytosis and production of effector molecules (cytokines and ROS), respectively[32,35,36,37]. Our evidence that MS4A4A-deficient macrophages show normal phagocytic properties but reduced Syk phosphorylation and impaired cytokine and ROS production indicates that MS4A4A is functionally relevant for the Syk-dependent signalling pathway in macrophages. In macrophages, MS4A4A expression was significantly increased by IL-4 and, intriguingly, glucocorticoids. In patients with Graves' disease treated with methylprednisolone, *MS4A4A* induction was observed in circulating monocytes, thus providing an *in vivo* confirmation of the regulation found *in vitro*. Glucocorticoid hormones are potent regulators

of immunity and inflammation and macrophages are a prime target for their action under physiological and pharmacological conditions[38]. Glucocorticoid hormones not only suppress inflammatory cytokines production, but also orchestrate tissue remodeling and reshape macrophage functions with the induction of anti-inflammatory molecules such as the IL-1 decoy receptor IL-1R2[39] and selected chemokines[40]. Moreover, glucocorticoid hormones have been suggested to set components of the innate immune system in an alert mode, priming for immediate/early responses to pathogens[38]. Given the coupling of MS4A4A with a microbial sensor, its induction could be a component of this early aspect of the pathophysiology of glucocorticoid hormones. Irrespective of its significance, monocyte expression of MS4A4A could serve as a biomarker of the response of mononuclear phagocytes to these agents.

Macrophages have been shown to promote activation of NK cell anti-tumoral activities through direct cell-cell contacts or soluble mediators, including IL-15 and IFN-β[41,42]. In this setting, recent evidence in a melanoma model indicates that macrophage recognition of tumor cell-associated molecular patterns via Dectin-1 is associated with reduction of tumor burden and metastatic spreading due to the activation of cytotoxic NK cells[13]. NK cells are known to play a major role in resistance against hematologic neoplasms, while their role in solid tumors is usually considered less relevant[43]. Recent results challenge this long held view by showing that inactivation of the NK cell checkpoint IL-1R8 unleashes NK cell mediated resistance against carcinogenesis at NK cell-rich anatomical sites, such as the liver and the lung[44]. In line with this general view, results reported here indicate that when macrophages are engaged via Dectin-1 with B16F1 melanoma cells, the absence of MS4A4A impairs their ability to upregulate CALHM6/INAM, secrete IFN-γ inducing cytokines, and trigger NK cell-mediated cytotoxic response, thus hampering NK cell ability to control tumor metastatization to the lung. Considering these evidences and the observation that MS4A4A is barely detectable in the

various subsets of circulating monocytes and induced during their differentiation to macrophages, we conclude that MS4A4A expression on TAM is likely required to support the interaction between NK cells and TAM observed in metastatic foci, where this cross-talk activates NK cells-mediated tumor cell killing. MS4A4A therefore does not contribute to the protumoral functions of TAM infiltrating primary tumors and conversely its expression in macrophages at metastatic sites is required for appropriate NK cell-mediated anti-tumoral functions. These results are well in line with previous results by us and others showing that the organ immunological context is indeed a key determinant of effective antitumor effector mechanisms[45], with divergent impact of immune manipulations on primary versus metastatic tumors[46,47]. There is evidence that the tissue contexture contributes to shaping the microenvironment of tumors originating in different organs[4]. Moreover, complex and diverse mechanisms orchestrate the formation of metastatic niches at sites of secondary localization of tumors[48]. Accordingly, it has long been known that immune mechanisms can have divergent impact of primary tumors and metastasis[3,47], as shown here for the MS4A4A-Dectin-1 interaction. Thus, in a therapeutic perspective, pathways of immune resistance at sites of secondary localization should be taken into account.

Several studies are ongoing with the aim of targeting TAM as a promising immune strategy to impact on tumor biology[3,49]. MS4A4A belongs to the same protein family of CD20 (also known as MS4A1)[14], whose targeting by specific monoclonal antibodies has proven to be effective for the treatment of hematological and autoimmune disorders[50]. Thus, from a translational perspective, our discovery of MS4A4A as a new M2/TAM marker raises the interesting possibility that it may represent a valid target for TAM depletion, though the anti-tumoral effect has to be balanced with the negative impact on metastasis spreading we have shown here. Finally, targeting the MS4A4A/Dectin-1

420 interaction may allow fine-tuning of uncontrolled, pathogen-triggered innate immune
421 responses.
422

ACKNOWLEDGMENTS

Authors thank C. Garlanda and M. Kallikourdis (Humanitas Clinical and Research Center IRCCS) for providing cDNAs of murine leukocyte subsets, T. Irimura (Juntendo University School of Medicine, Tokyo, Japan) and R. Giavazzi (Mario Negri Institute, Milan, Italy) for providing MC38 and SL4 cells. Technical assistance from A. Fontanini, C. Perrucchini, T. Schorn, R. Porte, and F. Pasqualini is acknowledged. A. Inforzato (Humanitas Clinical and Research Center IRCCS), A. Diefenbach (Charité - Universitätsmedizin Berlin, Germany), and L. Florin (University Medical Centre of the Johannes Gutenberg University, Mainz, Germany) are gratefully acknowledged for their support and discussion.

Financial support from Fondazione Cariplo (grant n. 2015-0564 to AM), Cluster Alisei (MEDINTECH CTN01_00177_962865 to AM), the European Research Council (grant no. 669415 - PHII to AM), the Italian Association for Cancer Research (AIRC IG-2016 grant n. 19014 to AM; AIRC 5X1000 grant n. 21147 to AM; AIRG IG-2016 grant n. 19213 to ML), Medical Research Council (Pathobiology of Early Arthrytis Cohort – PEAC grant n. 36661 to CP), and Arthritis Research UK Experimental Treatment Centre (grant n. 20022 to CP). IM was supported by a “Mario and Valeria Rindi” fellowship and a “Fellowship for abroad” from the Italian Foundation for Cancer Research, and by a European Federation of Immunological Societies-IL short-term fellowship. BS was supported by Ministero della Salute (progetto Finalizzata GR-2013-02356522). RSG was supported by a PhD studentship (PD/BD/114138/2016) from Fundação para a Ciência e Tecnologia, Purtugal. SKB was supported by core-funding from SIgN - A*STAR, Singapore. FT was supported by a fellowship from the A*STAR Research Attachment Program (ARAP), Singapore. SL was supported by Fondazione Beretta, Italy.

AUTHORS' CONTRIBUTIONS

IM, FT and MDP performed in vitro experiments; IM, BS and FT performed in vivo experiments; RS-G, MM and MSi provided support for in vivo and in vitro experiments; AD conducted the imaging analysis; DM and MSt provided support for analysis of molecular interactions; RC performed bioinformatics analysis; INS and YL performed gene expression experiments; SL, WV, MAB, AN, and TG performed histology; GM and CP provided access to patients samples; SKB, BB, CP, AM and ML contributed to the experimental design and supervision of the study.

COMPETING INTEREST STATEMENT

AM is a recipient of commercial research grants from Novartis, is a consultant/advisory board member for Novartis, Roche, Ventana, Pierre Fabre, Verily, AbbVie, Compugen, Macrophage Therapeutics, AstraZeneca, Biovelocita, BG Fund, Third Rock, and Verseau, is an inventor of patents related to PTX3 and other innate immunity molecules, and receives royalties for reagents related to innate immunity.

REFERENCES

1. Biswas, S.K. & Mantovani, A. Macrophage plasticity and interaction with lymphocyte subsets: cancer as a paradigm. *Nat Immunol* **11**, 889-896 (2010).
2. Murray, P.J. *et al.* Macrophage activation and polarization: nomenclature and experimental guidelines. *Immunity* **41**, 14-20 (2014).
3. Mantovani, A., Marchesi, F., Malesci, A., Laghi, L. & Allavena, P. Tumour-associated macrophages as treatment targets in oncology. *Nat Rev Clin Oncol* **14**, 399-416 (2017).
4. Ruffell, B., Affara, N.I. & Coussens, L.M. Differential macrophage programming in the tumor microenvironment. *Trends Immunol* **33**, 119-126 (2012).
5. Gabrilovich, D.I., Ostrand-Rosenberg, S. & Bronte, V. Coordinated regulation of myeloid cells by tumours. *Nat Rev Immunol* **12**, 253-268 (2012).
6. Martinez, F.O., Gordon, S., Locati, M. & Mantovani, A. Transcriptional profiling of the human monocyte-to-macrophage differentiation and polarization: new molecules and patterns of gene expression. *J Immunol* **177**, 7303-7311 (2006).
7. Martinez, F.O. *et al.* Genetic programs expressed in resting and IL-4 alternatively activated mouse and human macrophages: similarities and differences. *Blood* **121**, e57-69 (2013).
8. Varol, C., Mildner, A. & Jung, S. Macrophages: development and tissue specialization. *Annu Rev Immunol* **33**, 643-675 (2015).
9. Sanyal, R. *et al.* MS4A4A: a novel cell surface marker for M2 macrophages and plasma cells. *Immunol Cell Biol* **95**, 611-619 (2017).
10. Charrin, S. *et al.* Lateral organization of membrane proteins: tetraspanins spin their web. *Biochem J* **420**, 133-154 (2009).

11. Levy, S. & Shoham, T. The tetraspanin web modulates immune-signalling complexes. *Nat Rev Immunol* **5**, 136-148 (2005).
12. Howie, D. *et al.* MS4A4B is a GITR-associated membrane adapter, expressed by regulatory T cells, which modulates T cell activation. *J Immunol* **183**, 4197-4204 (2009).
13. Chiba, S. *et al.* Recognition of tumor cells by Dectin-1 orchestrates innate immune cells for anti-tumor responses. *Elife* **3**, e04177 (2014).
14. Adra, C.N. *et al.* Cloning of the cDNA for a hematopoietic cell-specific protein related to CD20 and the beta subunit of the high-affinity IgE receptor: evidence for a family of proteins with four membrane-spanning regions. *Proc Natl Acad Sci U S A* **91**, 10178-10182 (1994).
15. Hupp, K., Siwarski, D., Mock, B.A. & Kinet, J.P. Gene mapping of the three subunits of the high affinity FcR for IgE to mouse chromosomes 1 and 19. *J Immunol* **143**, 3787-3791 (1989).
16. Hollingworth, P. *et al.* Common variants at ABCA7, MS4A6A/MS4A4E, EPHA1, CD33 and CD2AP are associated with Alzheimer's disease. *Nat Genet* **43**, 429-435 (2011).
17. Greer, P.L. *et al.* A Family of non-GPCR Chemosensors Defines an Alternative Logic for Mammalian Olfaction. *Cell* **165**, 1734-1748 (2016).
18. Cruse, G. *et al.* The CD20 homologue MS4A4 directs trafficking of KIT toward clathrin-independent endocytosis pathways and thus regulates receptor signaling and recycling. *Mol Biol Cell* **26**, 1711-1727 (2015).
19. Ishibashi, K., Suzuki, M., Sasaki, S. & Imai, M. Identification of a new multigene four-transmembrane family (MS4A) related to CD20, HTm4 and beta subunit of the high-affinity IgE receptor. *Gene* **264**, 87-93 (2001).
20. Boucheix, C. & Rubinstein, E. Tetraspanins. *Cell Mol Life Sci* **58**, 1189-1205 (2001).

21. Hemler, M.E. Tetraspanin functions and associated microdomains. *Nat Rev Mol Cell Biol* **6**, 801-811 (2005).

22. Tarrant, J.M., Robb, L., van Spriel, A.B. & Wright, M.D. Tetraspanins: molecular organisers of the leukocyte surface. *Trends Immunol* **24**, 610-617 (2003).

23. Dombrowicz, D. *et al.* Allergy-associated FcRbeta is a molecular amplifier of IgE- and IgG-mediated in vivo responses. *Immunity* **8**, 517-529 (1998).

24. Polyak, M.J., Li, H., Shariat, N. & Deans, J.P. CD20 homo-oligomers physically associate with the B cell antigen receptor. Dissociation upon receptor engagement and recruitment of phosphoproteins and calmodulin-binding proteins. *J Biol Chem* **283**, 18545-18552 (2008).

25. Meyer-Wentrup, F. *et al.* Dectin-1 interaction with tetraspanin CD37 inhibits IL-6 production. *J Immunol* **178**, 154-162 (2007).

26. Taylor, P.R. *et al.* Dectin-1 is required for beta-glucan recognition and control of fungal infection. *Nat Immunol* **8**, 31-38 (2007).

27. Wuthrich, M., Deepe, G.S., Jr. & Klein, B. Adaptive immunity to fungi. *Annu Rev Immunol* **30**, 115-148 (2012).

28. Dambuza, I.M. & Brown, G.D. C-type lectins in immunity: recent developments. *Curr Opin Immunol* **32**, 21-27 (2015).

29. Goodridge, H.S. *et al.* Differential use of CARD9 by dectin-1 in macrophages and dendritic cells. *J Immunol* **182**, 1146-1154 (2009).

30. Brown, G.D. Dectin-1: a signalling non-TLR pattern-recognition receptor. *Nat Rev Immunol* **6**, 33-43 (2006).

31. del Fresno, C. *et al.* Interferon-beta production via Dectin-1-Syk-IRF5 signaling in dendritic cells is crucial for immunity to C. albicans. *Immunity* **38**, 1176-1186 (2013).

32. Brubaker, S.W., Bonham, K.S., Zanoni, I. & Kagan, J.C. Innate immune pattern recognition: a cell biological perspective. *Annu Rev Immunol* **33**, 257-290 (2015).

33. Rogers, N.C. *et al.* Syk-dependent cytokine induction by Dectin-1 reveals a novel pattern recognition pathway for C type lectins. *Immunity* **22**, 507-517 (2005).
34. Zanoni, I. *et al.* CD14 controls the LPS-induced endocytosis of Toll-like receptor 4. *Cell* **147**, 868-880 (2011).
35. Dennehy, K.M. *et al.* Syk kinase is required for collaborative cytokine production induced through Dectin-1 and Toll-like receptors. *Eur J Immunol* **38**, 500-506 (2008).
36. Herre, J. *et al.* Dectin-1 uses novel mechanisms for yeast phagocytosis in macrophages. *Blood* **104**, 4038-4045 (2004).
37. Underhill, D.M., Rossnagle, E., Lowell, C.A. & Simmons, R.M. Dectin-1 activates Syk tyrosine kinase in a dynamic subset of macrophages for reactive oxygen production. *Blood* **106**, 2543-2550 (2005).
38. Cain, D.W. & Cidlowski, J.A. Immune regulation by glucocorticoids. *Nat Rev Immunol* **17**, 233-247 (2017).
39. Colotta, F. *et al.* Interleukin-1 type II receptor: a decoy target for IL-1 that is regulated by IL-4. *Science* **261**, 472-475 (1993).
40. Kodelja, V. *et al.* Alternative macrophage activation-associated CC-chemokine-1, a novel structural homologue of macrophage inflammatory protein-1 alpha with a Th2-associated expression pattern. *J Immunol* **160**, 1411-1418 (1998).
41. Bellora, F. *et al.* The interaction of human natural killer cells with either unpolarized or polarized macrophages results in different functional outcomes. *Proc Natl Acad Sci U S A* **107**, 21659-21664 (2010).
42. Mattiola, I. *et al.* Priming of Human Resting NK Cells by Autologous M1 Macrophages via the Engagement of IL-1beta, IFN-beta, and IL-15 Pathways. *J Immunol* **195**, 2818-2828 (2015).

567 43. Gorelik, E., Wiltrout, R.H., Okumura, K., Habu, S. & Herberman, R.B. Role of NK
568 cells in the control of metastatic spread and growth of tumor cells in mice. *Int J*
569 *Cancer* **30**, 107-112 (1982).
570 44. Molgora, M., Barajon, I., Mantovani, A. & Garlanda, C. Regulatory Role of IL-1R8 in
571 Immunity and Disease. *Front Immunol* **7**, 149 (2016).
572 45. Molgora, M. *et al.* IL-1R8 is a checkpoint in NK cells regulating anti-tumour and anti-
573 viral activity. *Nature* **551**, 110-114 (2017).
574 46. Mantovani, A., Giavazzi, R., Polentarutti, N., Spreafico, F. & Garattini, S. Divergent
575 effects of macrophage toxins on growth of primary tumors and lung metastases in
576 mice. *Int J Cancer* **25**, 617-620 (1980).
577 47. Massara, M. *et al.* ACKR2 in hematopoietic precursors as a checkpoint of neutrophil
578 release and anti-metastatic activity. *Nat Commun* **9**, 676 (2018).
579 48. Noy, R. & Pollard, J.W. Tumor-associated macrophages: from mechanisms to
580 therapy. *Immunity* **41**, 49-61 (2014).
581 49. Majety, M., Runza, V., Lehmann, C., Hoves, S. & Ries, C.H. A drug development
582 perspective on targeting tumor-associated myeloid cells. *FEBS J* **285**, 763-776
583 (2018).
584 50. Franks, S.E., Getahun, A., Hogarth, P.M. & Cambier, J.C. Targeting B cells in
585 treatment of autoimmunity. *Curr Opin Immunol* **43**, 39-45 (2016).
586

FIGURE LEGENDS

Figure 1. MS4A4A expression and its regulation in human macrophages.

a-c) Flow cytometry analysis of MS4A4A surface expression on human leukocyte subsets (a), monocytes during M-CSF-dependent differentiation to macrophages (b), and differentiated macrophages treated for 18 h as indicated or not (M0) (c). Results are shown as mean ± SEM of relative Mean Fluorescence Intensity (MFI; fold on isotype). Two biologically independent experiments were performed, with each dot representing a biologically independent sample (a: 3 donors for $CD14^{hi}/CD16^{neg}$ monocytes, $CD14^{lo}/CD16^{pos}$ monocytes, NK, NKT, T, mDC, and pDC; 4 for $CD14^{dim}/CD16^{pos}$ monocytes, B, PMN; 8 for macrophages; b: 2 donors for day 7 after M-CSF treatment, 3 for monocytes and day 3 after M-CSF treatment; 4 for day 1 and 5 after M-CSF treatment; c: 3 donors). Statistical analysis by one-way ANOVA.

d) MS4A4A expression on human macrophages treated with IL-4 plus Dex (Dex+IL-4) or not (Medium) for 18 h. DAPI staining of nuclei is shown in blue. Immunofluorescence images are representative of one experiment out of three biologically independent performed.

e-f) Time-course of *MS4A4A* mRNA (e) and plasma membrane protein (f) in human macrophages treated with Dex for the indicated time. Results are shown as mean ± SEM of fold change (e) or relative MFI (f; fold change on M0). Two biologically independent experiments were performed (3 donors for e and 5 for f). Statistical analysis by two-tailed one sample Student's t test.

g) Expression levels of *MS4A4A* mRNA in monocytes isolated from three Graves' syndrome orbitopathy patients before and 6 h after injection with 1 g methylprednisolone. Results are shown as fold change on untreated cells (open columns).

h) Flow cytometry analysis of macrophage plasma membrane expression of MS4A4A and other indicated M2 markers (CD36, CD163, CD206) in resting conditions (-) or after exposure for 18 h to IL-4 plus M Dex (+).Two biologically independent experiments were performed (4 donors).

Figure 2. Macrophage expression of MS4A4A in human tissues.

MS4A4A expression on formalin fixed paraffin-embedded sections of human colon (a-c), lung (d-f), and skin (g-i). MS4A4A is visualized in brown (single staining in b-e-h, left and middle panels). In double-stained sections, MS4A4A expression (brown) was combined with CD163 (blue) in b-e-h right panels, CD1c (blue) in c, CD303 (blue) in f, and CD207 (blue) in i. Omission of primary antibodies was used as negative control (a-d-g panels). Magnification: 100X (a-d-f and b-e-h left panels; scale bar: 200 μm), 200X (c-f-i; scale bar: 100 μm) and 400X (b-e-h, middle and right panels; scale bar: 50 μm). One set of images out of five healthy tissues analyzed is shown.

Figure 3. MS4A4A expression is restricted to CD163$^+$ macrophages in inflamed synovium.

a and c) Representative immunofluorescence images of MS4A4A expression on formalin fixed paraffin-embedded sections of synovial tissue from early RA patients. MS4A4A staining is visualized in yellow, CD68 in green, CD3/CD20/CD138/CD163 in red. Nuclei were counterstained with DAPI and are visualized in blue. Matching isotype control antibodies were used as negative control. Magnification: 15X for upper panels (scale bar: 250 μm), and 40X for lower panels (scale bar: 70 μm). One set of images out of five RA patients analyzed is shown.

b) Percentage of synovial macrophages (CD68$^+$ cells) from early RA patients positive for MS4A4A and/or CD163, quantified by immunofluorescence in five RA patients.

Figure 4. MS4A4A is expressed in murine TAMs but is dispensable for primary tumor growth.

a-f) MS4A4A expression on formalin fixed paraffin-embedded sections of human colon adenocarcinoma (a-b), lung adenocarcinoma (c-d), and melanoma (e-f). MS4A4A is visualized in brown (single staining in a-c-e, left and middle panels). In double-stained sections, MS4A4A expression (brown) was combined with CD163 (blue) in a-c-e right panels, CD1c (blue) in b, CD303 (blue) in d, and CD207 (blue) in f. Magnification: 100X in a-c-e left panels (scale bar: 200 μm), 200X in b-d-f panels (scale bar: 100 μm), and 400X in a-c-e middle and right panels (scale bar: 50 μm). One set of images out of five cancer tissues analyzed is shown.

g) Expression levels of the *MS4A4A* mRNA in murine TAM isolated from B16F1 tumors, Lewis lung carcinoma (LLC) tumors, and human renal cancer cell A498 tumor xenografts. Data are normalized to actin and expressed as mean ± SEM of *MS4A4A* relative expression in TAMs compared to corresponding PECs, used as control. Results pooled data (4 mice per group) from one representative experiment out of three run in triplicate for A498 model and from one experiment (3 mice per group) for LLC and B16F1 models.

h) Tumor growth curve in *Ms4a4a*$^{-/-}$ (open symbol) and wild-type (closed symbol) mice upon s.c. injection of B16F1 melanoma cells. Results are shown as mean ± SEM. Two biologically independent experiments were performed (11 mice). No statistical difference at any time point by two-tailed unpaired Student's t test.

i-j) Tumor volume (i) and incidence (j) of 3-methylcholanthrene-induced fibrosarcoma in *Ms4a4a*$^{-/-}$ (open symbol) and wild-type (closed symbol) mice. Results are shown as mean ± SEM. Two biologically independent experiments were performed (16 mice). No statistical difference at any time point by two-tailed unpaired Student's t test.

Figure 5. MS4A4A and Dectin-1 associate in lipid rafts after zymosan engagement.

a-d) FLIM-FRET analysis of eGFP mean fluorescence lifetime in CHO-K1 cells expressing eGFP-MS4A4A alone (V) or in combination with mCherry-MS4A4A (6 for V and 7 for MS4A4A), mCherry-MS4A6A (6 for V and 4 for MS4A6A), mCherry-MS4A7 (7 for V and 6 for MS4A7), and mCherry-Dectin-1 (4 for V and 8 for Dectin-1). FRET efficiency (E) and Förster radius (R) are indicated. Results are shown as mean ± SEM.

e-h) Colocalization of MS4A4A and Dectin-1 in lipid rafts (stained with cholera toxin; CT-B) in human macrophages treated with 100 μg/ml zymosan. Panel e reports the kinetic of colocalization of MS4A4A and Dectin-1, panels f and g the kinetics of localization of MS4A4A and Dectin-1 in lipid rafts, respectively. Results are shown as mean ± SEM of the colocalization index (Manders coefficient) in 20÷78 cells from three donors analyzed. Error bars are included in symbols. Statistical analysis in comparison with time 0 was performed by one-way ANOVA. Images referring to the 30 min time point are shown in panel h, with nuclei counterstained with DAPI visualised in white. Scale bars: 10 μm.

i-l) STED analysis of MS4A4A and Dectin-1 in lipid rafts (stained with CT-B) in human macrophages treated (+) or not (-) for 15 min with 100 μg/ml zymosan alone or in combination with 5 mM MβCD. Panel i shows images from one experiment representative of two analyzed. Panels j to l report the colocalization rate (%) of MS4A4A in lipid rafts, Dectin-1 in lipid rafts, and MS4A4A and Dectin-1, respectively. Results are shown as mean ± SEM of the colocalization rate in 20÷33 cells from 2 donors analyzed. Scale bars: 5 μm. Statistical analysis by two-tailed unpaired (Mann-Whitney) Student's t test (j and k) and one-way ANOVA (l).

Figure 6. MS4A4A is required for Dectin-1 signalling.

Dectin-1 expression and function in BMDMs from wild-type (closed symbol) and *Ms4a4a*$^{-/-}$ (open symbol) mice.

690 a) Dectin-1 surface expression upon stimulation with 100 µg/ml zymosan (solid line) or 100
691 ng/ml LPS (dashed line). Results are shown as relative MFI (fold on isotype) mean ± SEM.
692 Five biologically independent experiments were performed (time 0: 15 wild-type and 25
693 *Ms4a4a*$^{-/-}$ mice; 5 min: 11 wild-type and 20 *Ms4a4a*$^{-/-}$ mice; 15 min: 4 wild-type and 5
694 *Ms4a4a*$^{-/-}$ mice; 30 min: 4 wild-type and 3 *Ms4a4a*$^{-/-}$ mice; 30 min with LPS: 6 wild-type
695 and 5 *Ms4a4a*$^{-/-}$ mice).
696 b) Binding of zymosan-FITC. Results are shown as MFI mean ± SEM (time 0, 5, and 15
697 min: 6 wild-type and 6 *Ms4a4a*$^{-/-}$ mice; 30 min: 4 wild-type and 4 *Ms4a4a*$^{-/-}$ mice).
698 c) Phagocytosis of *Aspergillus fumigatus* conidia-FITC. Results are shown as mean ± SEM
699 of percentage (left y-axis, solid lines) and relative MFI (fold on untreated; right y-axis,
700 dotted lines) of FITC^{+} cells gated on F4/80^{+} cells. Three biologically independent
701 experiments were performed. At all time points, 6 wild-type and 8 *Ms4a4a*$^{-/-}$ mice.
702 d-f) Phosphorylation of Syk (d), ERK (e), and p38 (f) after stimulation with 100 µg/ml
703 zymosan. Results are shown as relative MFI (fold on untreated) mean ± SEM. Five
704 biologically independent experiments for d (time 5: 4 wild-type and 5 *Ms4a4a*$^{-/-}$ mice; time
705 15: 8 wild-type and 12 *Ms4a4a*$^{-/-}$ mice), three for e (time 5: 4 wild-type and 7 *Ms4a4a*$^{-/-}$
706 mice; time 15: 4 wild-type and 5 *Ms4a4a*$^{-/-}$ mice), four for f (time 5: 4 wild-type and 4
707 *Ms4a4a*$^{-/-}$ mice; time 15: 4 wild-type and 8 *Ms4a4a*$^{-/-}$ mice). Statistical analysis by two-
708 tailed unpaired (Mann-Whitney) Student's t test.
709 g-h) Secretion of IL-6 (g) and TNF (h) after stimulation for 6 h with 100 µg/ml zymosan or
710 100 ng/ml LPS. Cytokine levels in untreated cells were below detection limit. Results are
711 shown as mean ± SEM. Four biologically independent experiments were performed (g: 7
712 wild-type and 7 *Ms4a4a*$^{-/-}$ mice for zymosan; 6 wild-type and 7 *Ms4a4a*$^{-/-}$ mice for LPS; h: 7
713 wild-type and 6 *Ms4a4a*$^{-/-}$ mice for zymosan, 7 wild-type and 8 *Ms4a4a*$^{-/-}$ mice for LPS).
714 Statistical analysis by two-tailed unpaired (Mann-Whitney) Student's t test.

i) ROS production after stimulation with 100 µg/ml zymosan. Results are shown as MFI mean ± SEM (6 wild-type and 6 *Ms4a4a*$^{-/-}$ mice). Statistical analysis by two-tailed unpaired Student's t test.

Figure 7. MS4A4A regulates Dectin-1 recognition and control of B16F1 metastasis

a) Flow cytometry analysis of WGA binding on B16F1 and B16F10 cells. Results are shown as representative dot plot (left) and mean ± SEM of relative MFI (fold on unstained; right). Six biologically independent experiments were performed (10 independent samples). Statistical analysis by two-tailed unpaired (Mann-Whitney) Student's t test.

b) Syk phosphorylation in BMDMs from *Ms4a4a*$^{-/-}$ (open symbol) and wild-type (closed symbol) mice primed for 18 h with 10 ng/ml GM-CSF and cocultured at 1:1 ratio with apoptotic B16F1 cells. Results are shown as relative MFI (fold on unstained) mean ± SEM. Three biologically independent experiments were performed (11 wild-type and 6 *Ms4a4a*$^{-/-}$ mice). Statistical analysis by two-tailed unpaired (Mann-Whitney) Student's t test.

c) Cytokine secretion by BMDMs from *Ms4a4a*$^{-/-}$ (open symbol) and wild-type (closed symbol) mice primed for 18 h with 10 ng/ml GM-CSF and cocultured with B16F1 cells for 6 h. Cytokine levels in untreated cells were below detection limit. Results are shown as mean ± SEM. Two biologically independent experiments were performed (6 wild-type and 6 *Ms4a4a*$^{-/-}$ mice). Statistical analysis by two-tailed unpaired (Mann-Whitney) Student's t test.

d-e) Number of metastatic foci in lungs from *Clec7a*$^{-/-}$ (open symbol) and wild-type (WT, closed symbol) mice upon i.v. injection of B16F1 (d) or B16F10 (e) cells. Results are shown as mean ± SEM. Three biologically independent experiments for B16F1 cells (9 wild-type and 16 *Clec7a*$^{-/-}$ mice), one for B16F10 cells (7 wild-type and 6 *Clec7a*$^{-/-}$ mice). Statistical analysis by two-tailed unpaired (Mann-Whitney) Student's t test.

f-g) Number of metastatic foci in lungs from *Ms4a4a*$^{-/-}$ (open symbol) and wild-type (WT, closed symbol) mice upon i.v. injection of B16F1 (f) or B16F10 (g) cells. Results are shown as mean ± SEM. Five biologically independent experiments for B16F1 cells (23 wild-type and 26 *Ms4a4a*$^{-/-}$ mice), three for B16F10 cells (12 wild-type and 15 *Ms4a4a*$^{-/-}$ mice). Statistical analysis by two-tailed unpaired (Mann-Whitney) Student's t test.

h) Number of metastatic foci in lungs from wild-type mice upon i.v. injection of B16F1 treated for 1 h with 25 U/ml N-glycosidase F (N-glyc, open symbol) or buffer (NT, closed symbol). Results are expressed as mean ± SEM. Two biologically independent experiments were performed (12 mice for NT, 11 for N-glyc). Statistical analysis by two-tailed unpaired (Mann-Whitney) Student's test.

Figure 8. Expression of MS4A4A in macrophages is required for NK-mediated Dectin-1-triggered protection against metastasis.

a-b) Representative images (a) and number (b) of lung metastasis in *Ms4a4a*$^{-/-}$ (open symbol) and wild-type (closed symbol) mice injected i.v. with B16F1 cells upon NK cell depletion by anti-NK1.1 treatment. Results are shown as mean ± SEM. Two biologically independent experiments were performed. Statistical analysis by one-way ANOVA and two-tailed unpaired Student's t test.

c) NK cell infiltrating the lungs of *Ms4a4a*$^{-/-}$ (open symbol) and wild-type (WT, closed symbol) mice injected i.v. with B16F1 cells. Results are shown as mean ± SEM of absolute numbers (n) of Live/CD45^{+}/CD3^{-}/NK1.1^{+} cells. Three biologically independent experiments were performed (9 wild-type and 6 *Ms4a4a*$^{-/-}$ mice). Statistical analysis by two-tailed unpaired Student's t test.

d) Degranulation of NK cells after engagement with B16F1 cells in the presence of splenocytes from *Ms4a4a*$^{-/-}$ (open symbol) and wild-type (WT, closed symbol) mice. Results are shown as mean ± SEM of percentage of CD107a^{+} NK cells gated on

766 Live/CD45^{+}/CD3^{-}/NK1.1^{+} splenocytes. Two biologically independent experiments were
767 performed (4 wild-type and 5 *Ms4a4a*$^{-/-}$ mice). Statistical analysis by two tailed unpaired
768 (Mann-Whitney) Student's t test.
769 e-h) Expression levels of *Calhm6* (e), *Il12p40* (f), *Il15* (g), and *Il18* (h) mRNA in *Ms4a4a*$^{-/-}$
770 (open symbol) and wild-type (WT, closed symbol) BMDMs primed with 10 ng/ml GM-CSF
771 cocultured for 24 h with B16F1 apoptotic cells. Results are shown as mean ± SEM of fold
772 of induction. Two biologically independent experiments were performed (f: 5 wild-type and
773 8 *Ms4a4a*$^{-/-}$ mice; g: 5 wild-type and 8 *Ms4a4a*$^{-/-}$ mice; h: 4 wild-type and 8 *Ms4a4a*$^{-/-}$ mice;
774 i: 4 wild-type and 4 *Ms4a4a*$^{-/-}$ mice). Statistical analysis by two-tailed unpaired Student's t
775 test.
776 i) IFN-γ production by NK cells after engagement with B16F1 cells in the presence of
777 splenocytes from *Ms4a4a*$^{-/-}$ (open symbol) and wild-type (WT, closed symbol) mice.
778 Results are shown as mean ± SEM of percentage of IFN-γ^{+} NK cells gated on
779 Live/CD45^{+}/CD3^{-}/NK1.1^{+} splenocytes. Two biologically independent experiments were
780 performed (5 wild-type and 6 *Ms4a4a*$^{-/-}$ mice). Statistical analysis by two tailed unpaired
781 (Mann-Whitney) Student's t test.
782

METHODS

Cells.

Human peripheral blood mononuclear cells were isolated from buffy coats of healthy donors and monocytes were obtained by serial centrifugation as described[6] and approved by the institutional Ethical Committee of the Humanitas Clinical and Research Center. Monoctes were treated for 7 days with 50 ng/ml recombinant human (rh) GM-CSF (Miltenyi Biotech) plus 40 ng/ml rhIL-4 (Peprotech) to obtain dendritic cells, and to 100 ng/ml rhM-CSF (R&D Systems) to obtain macrophages. Macrophages were activated *in vitro* by 18 h incubation with either 100 ng/ml *055:B5* LPS (Sigma-Aldrich) plus 20 ng/ml rhIFN-γ (Peprotech), 20 ng/ml rhIL-10 (Miltenyi Biotech), 10 ng/ml rhTGF-β (Miltenyi Biotech), 10^{-6} M dexamethasone (Dex; Sigma-Aldrich), 20 ng/ml rhIL-4, or 10^{-6} M Dex plus 20 ng/ml IL-4. Murine bone marrow-derived macrophages (BMDMs) were generated by 6 days of culture with 20 ng/ml recombinant murine (rm) M-CSF (Miltenyi Biotech) and were cultured for 18 h with 100 ng/ml LPS plus 20 ng/ml rmIFN-γ (R&D Systems) or 20 ng/ml rmIL-4 (R&D Systems). TAMs were isolated from s.c. B16F1 (0.1×10^6) or Lewis lung carcinoma (LLC; 1×10^6) tumors into C57BL/6J (Charles River Laboratories) or A498 human renal tumor cells (1×10^6) grown in NOD/scid/IL-2R-γ^{null} mice (NOD.Cg-*Prkdc*^{scid}*Il2rg*^{tm1Wjl}/SzJ; Jackson Laboratory). After mice were sacrificed (day 14 for LLC tumors, day 18 for A498 tumors, day 20 for B16F1 tumors), tumors were harvested and disaggregated. Peritoneal exudate macrophages (PECs) were collected by peritoneal lavage. Tumor suspension cells and PECs were stained for F4/80 and CD11b and F4/80$^+$/CD11b$^+$ TAMs and PECs were sorted using an Influx flow sorter (BD Bioscience) and immediately lysed for RNA extraction. B16F1 and B16F10 cells were cultured in RPMI 1640, 10% FBS, 1% L-glutamine, 1% penicillin/streptomycin, 1% HEPES (Lonza). B16F1

808 cells were induced to apoptosis by 5 min heat-shock at 65°C followed by 5 min on ice.
809 MC38 cells were cultured in Dulbecco's modified Eagle medium (DMEM; Lonza), 10%
810 FBS, 1% L-glutamine, 1% penicillin/streptomycin, 1% sodium pyruvate, 1% non-essential
811 amino acids (Lonza). SL4 cells were cultured in DMEM:F12 (1:1) medium (Lonza), 10%
812 FBS, 1% L-glutamine, 1% penicillin/streptomycin. Chinese hamster ovary (CHO-K1) cells
813 were grown in DMEM, 10% FBS, 100 U/ml penicillin/streptomycin, and 25 mM HEPES pH
814 7.2 (Gibco). Transfectants were obtained by lipofection with Lipofectamine 2000 according
815 to manufacturer's instructions, and selected with 650 μg/ml G418 (Invitrogen).
816
817 **Patients' samples.**
818 Monocytes from patients with active severe Graves orbitopathy were collected before and
819 6 h after the first i.v. infusion of 1 g methylprednisolone. A signed informed consent for
820 blood/serum collection and storage and for its use for research purposes was obtained by
821 the Endocrinology Unit, Fondazione IRCCS Ca' Granda Policlinico. In agreement with the
822 institutional policy, the Ethical Committee approval was not required, as patients did not
823 undergo tests or therapies other than those routinely proposed for their specific disease.
824 Rheumatoid arthritis (RA) synovium samples were retrieved from early (<12 months
825 symptoms) patients fulfilling the ACR/EULAR 2010 criteria[51] for RA diagnosis, recruited
826 into the Pathobiology of Early Arthritis Cohort (PEAC; http://www.peac-
827 mrc.mds.qmul.ac.uk/) at Bart's Health NHS Trust in London. After obtaining written
828 informed consent, patients underwent an ultrasound-guided needle synovial biopsy of the
829 most inflamed accessible joint[52]. Synovial tissue samples were immediately fixed in 4%
830 formaldehyde (Merck) and subsequently paraffin-embedded. The study was approved by
831 the institutional Ethical Committee (No. 05/Q0703/198). Histological analysis of normal and
832 tumoral tissue samples was performed on material obtained from the Surgical Pathology
833 Unit, ASST-Spedali Civili in Brescia. Experiments performed on archival material were

834 approved by the institutional Ethical Committee (WV-Immunocancer 2014 to WV, IRB
835 code NP906). When requested, an informed consent was obtained from all participants.
836
837 **Immunohistochemical and immunofluorescence analysis.**
838 MS4A4A expression was analyzed on 4-μm formalin-fixed paraffin-embedded sections of
839 normal tissues (skin, lung, colon) and corresponding neoplastic samples (five melanomas,
840 five lung adenocarcinomas, five colon adenocarcinomas) by staining with anti human
841 MS4A4A (rabbit polyclonal, dilution 1:4.000; Sigma-Aldrich) and revealing using Novolink
842 Polymer (Leica Biosystems) as secondary reagent. The chromogen reaction was
843 developed using diaminobenzidine. For double immunostains, MS4A4A was combined
844 with CD1c (clone OTI2F4; Abcam), CD163 (clone 10D6; Thermo Fisher Scientific), CD207
845 (clone 12D6; Vector Laboratories), and CD303 (clone 124B3.13; Dendritics). The second
846 antibody reactivity was detected using a Mach 4 alkaline phosphatase system with Ferangi
847 Blue (Biocare Medical) as chromogen. Slides were counterstained with hematoxylin.
848 Omission of primary antibody was also performed as control staining. Immunostained
849 sections were photographed using the DP73 Olympus digital camera mounted on the
850 Olympus BX60 microscope and analyzed by the acquisition software CellSens Standard.
851 Images were then processed using Adobe Photoshop Cs4 Portable. MS4A4A expression
852 on inflamed synovium was performed on 3-μm formalin-fixed paraffin embedded sections
853 obtained from five patients by multiplex immunofluorescence staining using a tyramide
854 signal amplification protocol and an anti-MS4A4A rabbit polyclonal anti human antibody
855 (dilution 1:2000; Sigma-Aldrich) in combination with CD68 (mouse anti human IgG1, clone
856 KP1; Dako), CD163 (mouse anti human IgG1, clone 10D6; Leica Biosystems), CD3
857 (mouse anti human IgG1, clone F7.2.38; Dako), CD20 (mouse anti human IgG2a, clone
858 L26; Dako), and CD138 (mouse anti human IgG1, clone MI15; Dako). Matching isotypes
859 were used as controls. Nuclei were counterstained with 4',6-diamidino-2'-phenylindole

(DAPI, 300 nM; Invitrogen) and mounted with ProLong Antifade Mountant (Thermo Fisher Scientific). Sections were imaged with the digital slide scanner Nanozoomer S60 (Hamamatsu Photonics). The quantification of CD68/MS4A4A/CD163^{+} cells was performed using the cell count plugin of the Image J software. TAMs and NK cells infiltrating experimental metastasis were analyzed on frozen sections (10 μm thick) obtained from tissue blocks of B16F1 metastasis-bearing lungs. Sections were thawed and fixed with 4% PFA for 5 min, washed and incubated for 15 min in PBS supplemented with 0.05% Tween-20, 2% BSA, 5% donkey serum (Sigma-Aldrich), and incubated for 1 h with purified polyclonal goat anti mouse NKp46 (R&D System), rat anti mouse F4/80 (Serotech), and rabbit anti mouse Ki-67 (Cell Signalling). After extensively wash, sections were incubated for 1 h with Alexa Fluor (488, 568, 647)-conjugated species-specific cross-adsorbed detection antibodies (Molecular Probes). Nuclei were stained using DAPI. Sections were mounted with 20 μl FluorSave reagent (Calbiochem). Fluorescent high-resolution images were acquired with a Leica SP8 STED 3X confocal microscope (Leica HC PL APO 60X/1.40 oil STED white objective system) and analyzed by LAS-X software.

Animal colonies.

Wild-type C57BL/6J mice were obtained by Charles River Laboratories (Calco, Italy). Mice with macrophage-specific *Ms4a4a* inactivation in C57BL/6J background were achieved breading mice carrying floxed *Ms4a4a* alleles (*Ms4a4a*$^{fl/fl}$; Ozgene) with mice expressing Cre under the control of the promoter of the *Lys* gene, encoding for the myeloid-restricted lysozyme M protein (*Lys*$^{Cre/+}$; B6.129P2-*Lyz2*$^{tm1(cre)Ifo}$/J from Jackson Laboratory). *Ms4a4a*$^{fl/fl}$*Lys*$^{Cre/+}$ mice (here indicated as *Ms4a4a*$^{-/-}$) were born in Mendelian ratios, reproduced normally, and did not show significant differences in body weight compared to control floxed littermates (*Ms4a4a*$^{fl/fl}$*Lys*$^{+/+}$, here used as wild-type animals). *Ms4a4a*$^{-/-}$ mice were co-housed with littermates in individually ventilated cages in a specific

886 pathogen-free/viral antibody-free animal facility at Humanitas Clinical and Research
887 Center. Mice in C57BL/6J background with *Dectin-1* inactivation (*Clec7a*$^{-/-}$; B6.129S6-
888 *Clec7a*^{tm1Gdb}/J) were obtained by Jackson Laboratory. To obtain double-deficient mice
889 (here indicated as *Ms4a4a*$^{-/-}$*Clec7a*$^{-/-}$), Clec7a$^{-/-}$ mice were bred with
890 *Ms4a4a*$^{fl/fl}$/ubiquitinC$^{Cre/+}$ animals (B6.Cg$^{Tg(UBC-cre/ERT2)1Ejb}$/2J from Jackson Laboratory).
891 Animals were housed in ventilated cages in a specific pathogen-free/viral antibody-free
892 animal facility at Humanitas Clinical and Research Center. Experiments were performed
893 using sex- and age-matched mice.
894
895 **Experimental models.**
896 The 3-methylcholanthrene (3-MCA)-induced tumor model was performed with 100 μg 3-
897 MCA as previously described[53]. In the melanoma B16F1 model, tumor dimension was
898 monitored in mice s.c. injected with 0.1 × 10^6 B16F1 cells as previously described[13]. Lung
899 metastasis were analyzed in the lungs 10 days after i.v. injection with 0.3 × 10^6 B16F1 or
900 B16F10 cells and 14 days after i.v. injection with 0.3 × 10^6 SL4 cells. To visualize
901 metastasis, lungs from mice injected with SL4 were fixed and stained over night with
902 Bouin's Solution (Histoline). Liver metastasis were analyzed 14 days after i.s. injection with
903 0.25 × 10^6 MC38 cells. For NK cell depletion in the melanoma model, mice were i.p.
904 injected with 200 μg anti-NK1.1 (BioXcell) or its isotype control 3 days before and 100 μg
905 anti-NK1.1 or isotype control 3 and 7 days after B16F1 cells injection and metastasis were
906 evaluated at day 10. For NK cell depletion in the colon carcinoma model, mice were i.p.
907 injected with 200 μg anti-NK1.1 (BioXcell) or its isotype control 5 and 3 days before and 3
908 and 7 and 10 days after MC38 cells injection and metastasis were evaluated at day 12.
909 Animal procedures were reviewed and approved by the institutional Ethical Committee at
910 Humanitas Clinical and Research Center and were in accordance with national (D.L. N.

116, G.U. suppl. 40, 18-2-1992 and N. 26, G.U. 4-3-2014) and international laws and policies (EEC Council Directive 2010/63/EU, OJ L 276/33 22-9-2010; National Institutes of Health Guide for the Care and Use of Laboratory Animals, US National Research Council, 2011). The study was approved by the Italian Ministry of Health (approvals n. 89/2013-B issued on the 8/4/2013, 6B2B3.N.ERY issued on 06/12/2017, and 949/2018-PR issued on the 20/12/2018).

Split-ubiquitin assay.

The split-ubiquitin assay was performed as previously described[12]. Briefly, a split-ubiquitin NubG-X library, derived from monocyte-derived human macrophages treated with 10^{-6} M Dex, was directionally cloned into the prey vector pBT3-N and the bait protein MS4A4A cDNA was cloned into the bait vector pBT3-STE, in which the LexA-VP16-Cub cassette is fused to the N-terminus. The yeast strain NMY51 (MATa his3-200 trp1–901 leu2–3,112 ade2 LYS2::(lexAop)4-HIS3 ura3::(lexAop)8-LacZ ade2::(lexAop)8-ADE2 GAL4) was transformed using standard procedures . Transformants were grown on selective medium lacking leucine, tryptophan, histidine and adenine, with addition of 20 mM 3-amino-1,2,4-triazole. Positive clones were sequenced by colony PCR (pPR3N-FOR: 5′-GTCGAAAATTCAAGACAAGG-3′; pPR3N-REV: 5′-AAGCGTGACATAACTAATTAC-3′). Library plasmids were isolated from positive clones and retransformed into NMY51 to test bait dependency. Prey sequences activating the histidine and adenine reporters in the presence of MS4A4A and not the empty pBT3-STE vector were considered as potential MS4A4A interactors.

Flow cytometry.

For direct multi-color flow cytometry (FACS Canto II and LRS Fortessa; BD Bioscience), cells were incubated for 30 min at 4°C with directly conjugated anti-human or anti-mouse

protein antibodies (Supplementary Tables 1 and 2, respectively, Life Science Reporting Summary) and their appropriate isotype controls. Live/dead cell discrimination was performed staining with the Zombie Aqua Fixable Viability Kit (BioLegend). For MS4A6A and MS4A7 surface staining, purified MS4A6A (Abnova) and MS4A7 (Novusbio) antibodies were used as primary antibodies and anti human IgG-Alexa Fluor 488 (Invitrogen) as secondary antibody. Wheat germ agglutinin Alexa Fluor 594-conjugated (WGA; ThermoFisher) was used to detect N-acetylglucosamine residues on the surface of tumor cells. To block Fc receptors, a purified anti mouse CD16/CD32 (BioLegend) was used. For intracellular staining, cells were permebilized and fixed using the FoxP3/Transcription Factor Staining Buffer Set (eBioscience). Phosphoproteins were detected as previously described[29] using the anti-phospho-Syk-Tyr525/526 antibody (Cell Signalling) and the anti-phospo-p38-Thr180/Tyr182 antibody (Cell Signalling) as primary antibodies and an anti rabbit IgG Alexa Fluor 647 as secondary antibody (Invitrogen) or the directly conjugated anti-phospho-ERK Alexa Fluor 647 antibody (BD Pharmigen), according to protocols recommended by the manufacturers. To analyze immune cell infiltration, lungs were incubated for 1 h at 37°C in 1% DNAse I in HBSS supplemented with 1 mg/ml collagenase D (Roche) and then for 10 min in 5 mM EDTA on ice. The cell suspension was passed through a 70 μm filter, red cells were lysed with ACK (Lonza), and then cells were stained and analyzed by flow cytometry. Data were analyzed with FACS Diva (BD) and Flow Jo (Treestar) software. Gating strategies are reported in Supplementary Note.

Imaging analysis.

Freshly isolated human monocytes were differentiated to macrophages directly on 14-mm diameter cover glasses (Menzel-Gläser) in 24-well plates and treated as described above. Cells were fixed with 4% PFA (Euromedex). For intracellular staining, cells were

963 permeabilized with 0.1% Triton X-100 (Sigma-Aldrich), 2% BSA (Biosera), 5% goat serum
964 (Dako) in PBS. Cells were then incubated for 18 h with a purified mouse anti human
965 MS4A4A MoAb (R&D System) and a purified goat anti human Dectin-1 polyclonal (R&D
966 System) and then for 1 h with Alexa Fluor (488, 647)-conjugated species-specific cross
967 adsorbed detection antibodies (Molecular Probes). Nuclei were stained using DAPI. Lipid
968 rafts were stained with the Vybrant Lipid Raft Labeling Kit, based on the cholera toxin
969 subunit B (CT-B) labeled with the red-fluorescent Alexa Fluor 594 dye (Molecular Probes),
970 following the manufacturer protocol. High-resolution images (1024 × 1024 pixels) were
971 acquired with an Olympus Fluoview FV1000 laser scanning confocal microscope with 60X
972 (N.A. 1.4) plan-apochromat oil immersion objective (Olympus) and analyzed with ImageJ
973 software (NIH). Quantitative colocalization and statistical analysis were performed with
974 Imaris Coloc 4.2 (Bitplane AG) software and FV1000 1.6 colocalization software
975 (Olympus) and ImageJ Coloc2 plugin. Representative images were smoothed with a
976 Gaussian filter and upscaled with bicubic interpolation (ImageJ). For STED microscopy,
977 human macrophages were stained with purified mouse anti human MS4A4A monoclonal
978 Ab (R&D System) and a purified goat anti human Dectin-1 polyclonal (R&D System) and
979 then for 1 h with Alexa Fluor (568, 647)-conjugated species-specific cross-adsorbed
980 detection antibodies (Molecular Probes). Lipid rafts were stained with the Vybrant Lipid
981 Raft Labeling Kit, based on the CT-B labeled with the green-fluorescent Alexa Fluor 488
982 324 dye (Molecular Probes), following the manufacturer protocol. Mowiol was used as
983 mounting medium. Alexa Fluor 488, 568 and 647 were excited with a 400 Hz white light
984 laser tuned at 485/493, 561/569 and 635/643 nm, respectively, and emission was
985 collected at 505-550, 580-620, and 650-700 nm, respectively. A gating between 0.4 to 7 ns
986 was applied to avoid collection of reflection and autofluorescence and sequential
987 acquisition was applied to avoid fluorescence overlap. The 775 nm CW-depletion laser
988 (30% of power; ≈90 mW) was used for Alexa Fluor 488, 568 and 647 excitations. STED

analysis was performed on ROI corresponding to the traced freehand area of the image of a single cell (3-5 ROIs per image) and *xyz* images (1928 × 1928 px; px size, 0.05 μm; vx size, 0.2 μm) were acquired in a *z*-stack (30-40 images; 0.2 μm slice) with a Leica SP8 STED 3X confocal microscope system adopting a Leica HC PL APO 100x/1.40 oil STED white objective at 706-929 mAU. CW-STED and gated CW-STED were applied to Alexa Fluor 488 and Alexa Fluor 568 and 647, respectively. A linear background subtraction was applied to all *z*-stack STED images. The colocalization rate was measured with the LASX software after a maximum intensity projection of the non-deconvolved images. Collected images were deconvolved with Huygens Professional software. To evaluate the interaction between MS4A4A and its putative partners, we investigated by Fluorescence Lifetime Imaging Microscopy (FLIM) the Fluorescence Resonance Energy Transfer (FRET) from an excited MS4A4A-eGFP donor molecule to ground state proximal acceptor molecules chimerized to the fluorescent protein mCherry[54]. To this purpose, eGFP-MS4A4A and mCherry chimerized candidate partners were cotransfected in 2 × 10^5 CHO-K1 cells seeded onto poly-L-lysine treated coverslips, cells were fixed, irradiated with a 830 nm light to excite the donor, and imaged using a TriM Scope II two photon laser scanning microscope (LaVision Biotec) equipped with a 60X water immersion lens (LUMFL60x; Olympus). Light was separated using a IR700 long pass filter and detected with the FLIM X16 TCSPC module 350 (LaVision Biotec). FLIM data were fitted with single exponential and background correction using Imspector Pro (LaVision Biotech). FRET efficiency (E) and Förster radius (R), which express the distance between the molecules, are reported.

Gene expression analysis.

For real-time PCR assay (qPCR), cells were lysed with QIAzol Reagent (Qiagen) and total RNA was extracted using miRNeasy mini kit (Qiagen). RNA was converted in cDNA using the High-Capacity cDNA Reverse Transcription Kit (Applied Biosystems) and quantification

of the transcripts reported in Supplementary Table 3 was performed following the recommended protocols for SYBR Green Master Mix (Applied Biosystems). Results were normalized on human *GAPDH* or murine *Gapdh*. qPCR was performed with the ViiA™ 7 Real-Time PCR System (Applied Biosystems). To determine *MS4A4A* gene expression levels in different human tissues and cells lines and in different cancer types, the Laboratory for Systems Biology and Medicine RefExA database (http://sbmdb.genome.rcast.u-tokyo.ac.jp/refexa/main_search.jsp) and the Cancer Genome Atlas database (TCGA; https://doi.org/10.7908/C11G0KM9) through the Firebrowse repository (http://firebrowse.org/) were used. Gene expression levels as rsem values were downloaded and distribution boxplots were performed using the ggplot2 R package version 2.2.1. Correlation between *MS4A4A* and TAM markers transcripts were performed using the 'rcorr' function implemented in Hmisc R package version 4.0.3 adopting the Pearson's correlation method. Significant correlations ($p < 0.05$) were plotted using the NMF R package version 0.20.6. Genes with a not significant correlation show a coefficient equal to zero. Mentioned source data are provided in Supplementary Fig. 3.

NK cell functional assays.

NK cell degranulation was investigated by CD107a surface expression, as previously reported[42]. Briefly, splenocytes isolated from *Ms4a4a*$^{-/-}$ and wild-type mice were treated for 18 h with 100 ng/ml rmIL-2 and co-cultured for 4 h with B16F1 or B16F10 cells (E:T ratio 12:1). Percentage of CD107a^{+} NK cells (Live/CD45^{+}/CD3^{-}/NK1.1^{+}) was analyzed by flow cytometry. IFN-γ production was investigated on splenocytes isolated from *Ms4a4a*$^{-/-}$ and wild-type mice treated for 12 h with 50 ng/ml rmIL-2 and co-cultured for 4 h with B16F1 and additional 2 h with Golgi plug (BD Pharmingen). Percentage of IFN-γ^{+} NK cells (Live/CD45^{+}/CD3^{-}/NK1.1^{+}) was analyzed by flow cytometry.

Macrophage functional assays.

To study Dectin-1 functional activities, BMDMs were primed for 18 h with 10 ng/ml GM-CSF and treated with 100 μg/ml zymosan (InvivoGen), 100 μg/ml depleted zymosan (InvivoGen), 100 μg/ml curdlan (Wako Chemicals), 100 ng/ml LPS, 100 ng/ml PMA (Sigma-Aldrich), 100 ng/ml Pam3Cys (Enzo Life Science), 20 μg/ml fluorescein-conjugated zymosan bioparticles (Molecular Probes), or 5×10^6 *Aspergillus fumigatus* conidia-FITC. To deplete lipid rafts, macrophages were treated for 15 min with 100 μg/ml zymosan alone or in combination with 5 mM methyl-β-cyclodextrin (MβCD; Sigma-Aldrich). ROS production was investigated using the CellRox Deep Red reagent (Life Technologies) according to the manufacturer's instructions. Live-cell widefield microscopy was performed monitoring fluorescence at 350ex/461em (Hoechst) and 640ex/665em (CellROX) with a Cell-R epi-fluorescence microscope (Olympus). ROI were analyzed using the Xcellence software (Olympus). Secreted cytokines were measured by ELISA (Duoset; R&D System).

Statistical analysis.

Results were expressed as means ± SEM from multiple independent experiments. One-way ANOVA and two-tailed Student's *t* test were performed using Prism (GraphPad) and/or Excel (Microsoft) software. ROUT test was applied to determine outliers.

Data availability.

The data that support the findings of this study are available from the corresponding author upon reasonable request. *Ms4a4a*$^{fl/fl}$ animals have been developed by the research team and are available after evaluation of potential conflict of interest upon MTA.

Methods-only references.

51. Aletaha, D. *et al.* 2010 Rheumatoid arthritis classification criteria: an American College of Rheumatology/European League Against Rheumatism collaborative initiative. *Arthritis Rheum* **62**, 2569-2581 (2010).
52. Kelly, S. *et al.* Ultrasound-guided synovial biopsy: a safe, well-tolerated and reliable technique for obtaining high-quality synovial tissue from both large and small joints in early arthritis patients. *Ann Rheum Dis* **74**, 611-617 (2015).
53. Bonavita, E. *et al.* PTX3 is an extrinsic oncosuppressor regulating complement-dependent inflammation in cancer. *Cell* **160**, 700-714 (2015).
54. Millington, M. *et al.* High-precision FLIM-FRET in fixed and living cells reveals heterogeneity in a simple CFP-YFP fusion protein. *Biophys Chem* **127**, 155-164 (2007).

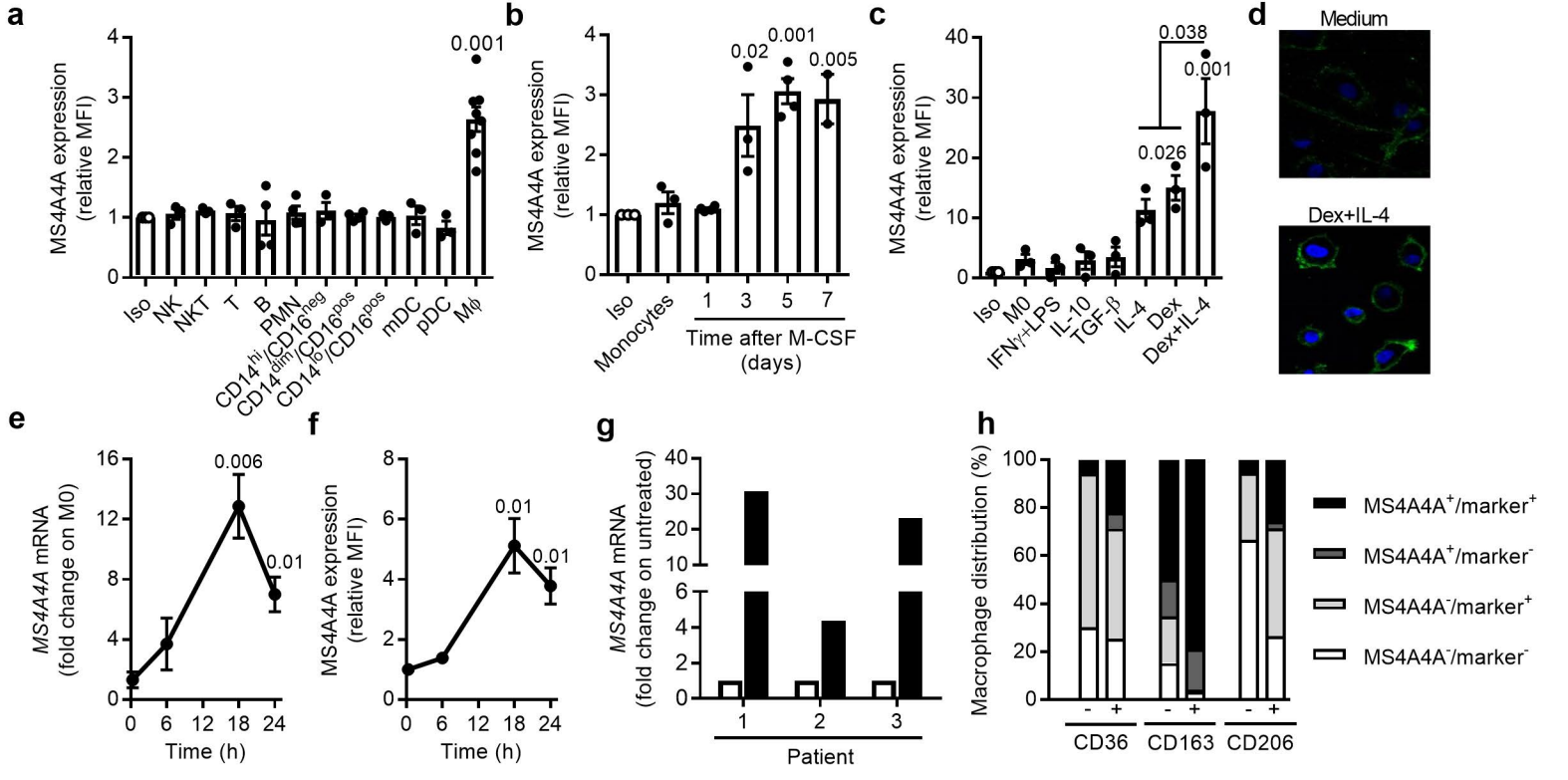
a
MS4A4A expression (relative MFI)
0.001
Iso
NK
NKT
T
B
PMN
CD14bri/CD16neg
CD14dim/CD16pos
CD14+/CD16pos
mDC
pDC
Mϕ
b
MS4A4A expression (relative MFI)
0.02
0.001
0.005
Iso
Monocytes
1
3
5
7
Time after M-CSF (days)
c
MS4A4A expression (relative MFI)
0.038
0.001
0.026
Iso
M0
IFNγ+LPS
IL-10
TGF-β
IL-4
Dex
Dex+IL-4
d
Medium
Dex+IL-4
e
MS4A4A mRNA (fold change on M0)
0.006
0.01
Time (h)
f
MS4A4A expression (relative MFI)
0.01
0.01
Time (h)
g
MS4A4A mRNA (fold change on untreated)
Patient
h
Macrophage distribution (%)
MS4A4A+/marker+
MS4A4A+/marker-
MS4A4A-/marker+
MS4A4A-/marker-
CD36
CD163
CD206

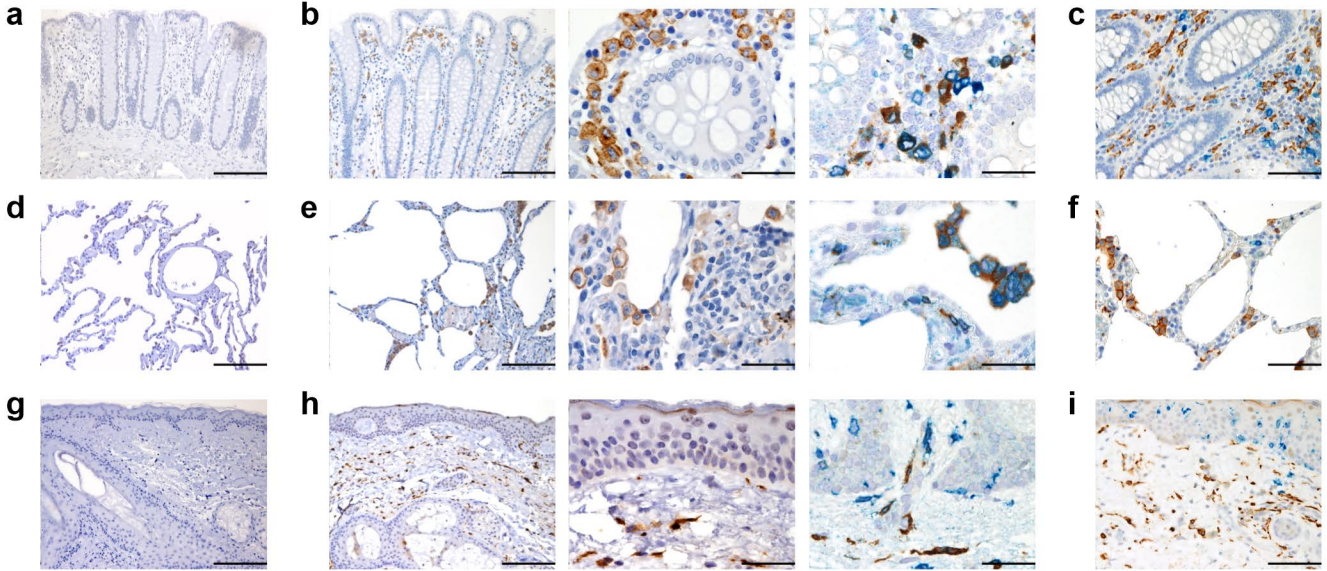
a
b
c
d
e
f
g
h
i

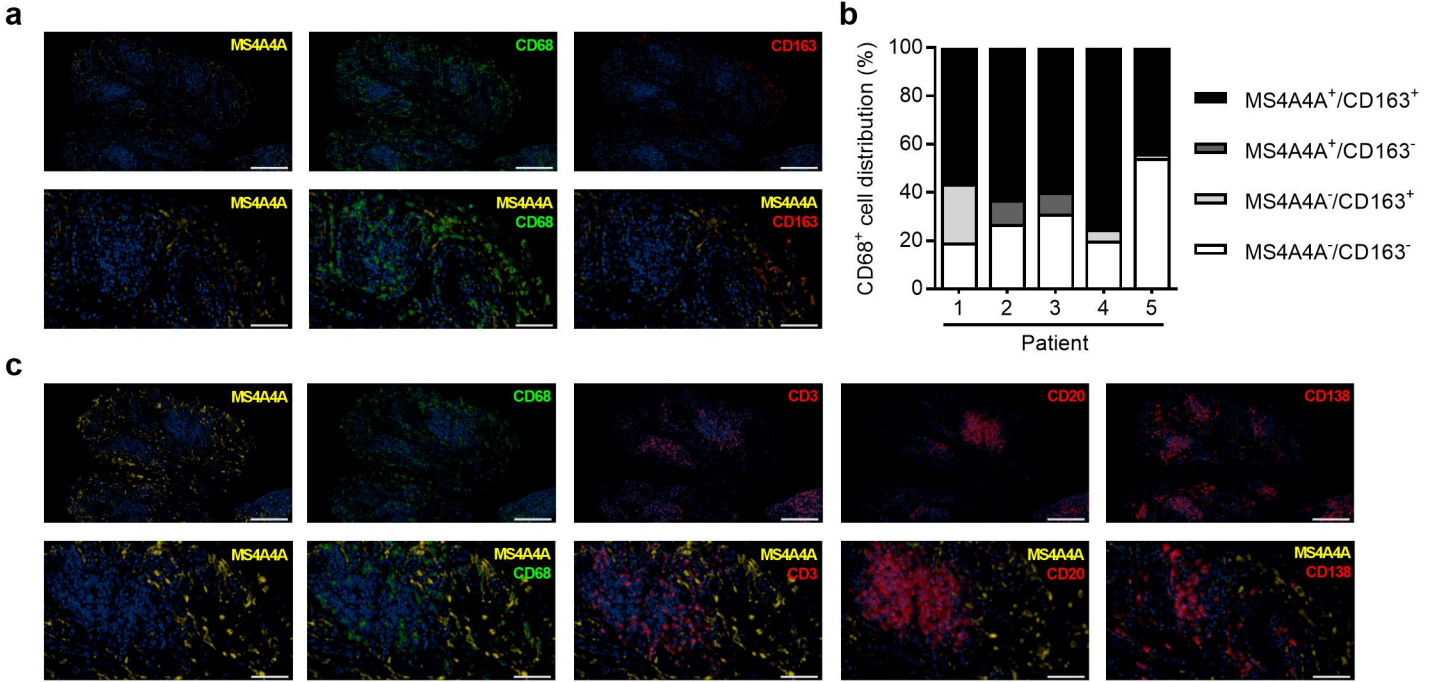
a
MS4A4A
CD68
CD163
MS4A4A
MS4A4A
CD68
MS4A4A
CD163
b
CD68+ cell distribution (%)
100
80
60
40
20
0
1
2
3
4
5
Patient
MS4A4A+/CD163+
MS4A4A+/CD163-
MS4A4A-/CD163+
MS4A4A-/CD163-
c
MS4A4A
CD68
CD3
CD20
CD138
MS4A4A
MS4A4A
CD68
MS4A4A
CD3
MS4A4A
CD20
MS4A4A
CD138

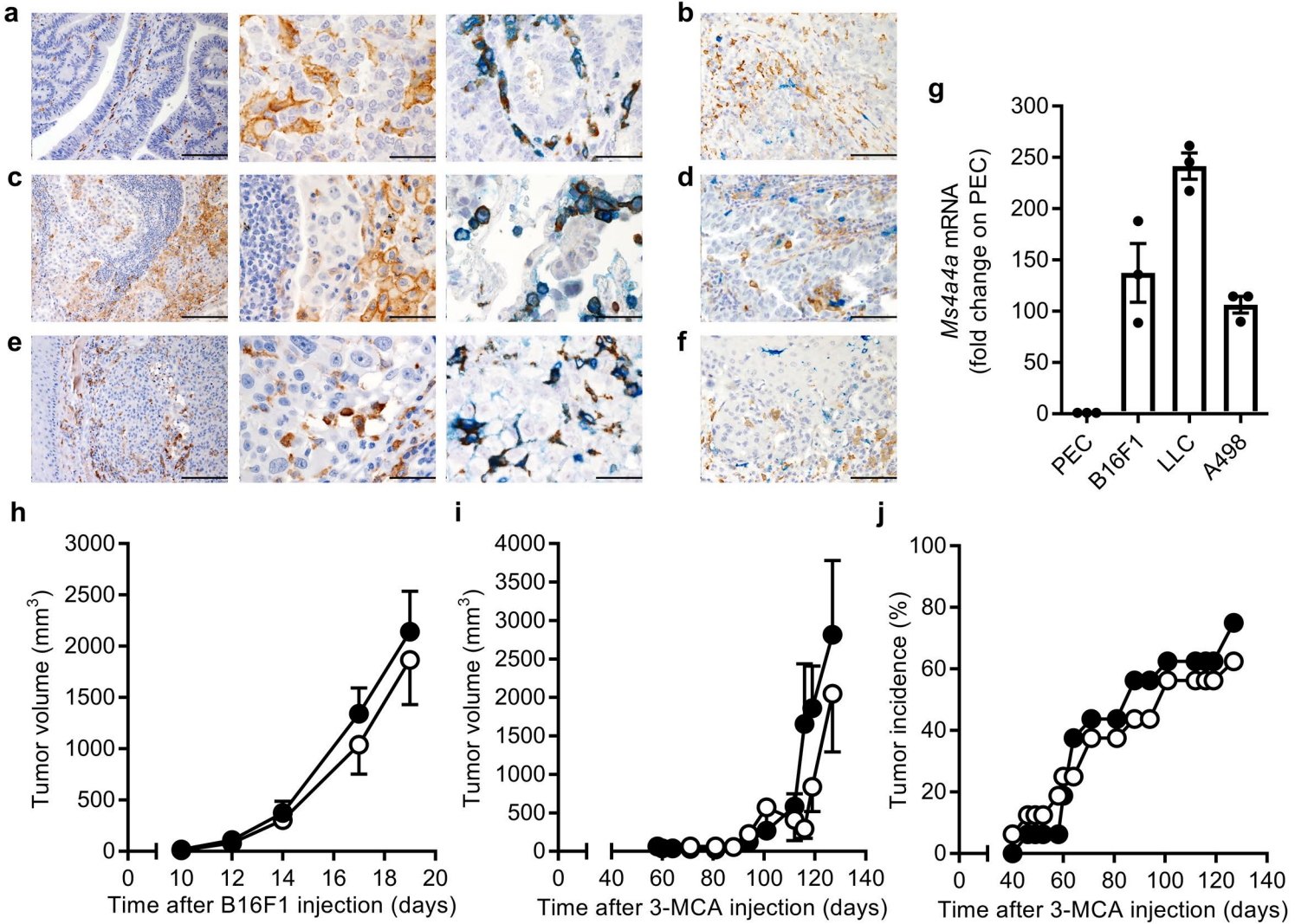
a
b
c
d
e
f
g
Ms4a4a mRNA (fold change on PEC)
300
250
200
150
100
50
0
PEC
B16F1
LLC
A498
h
Tumor volume (mm3)
3000
2500
2000
1500
1000
500
0
0
10
12
14
16
18
20
Time after B16F1 injection (days)
i
Tumor volume (mm3)
4000
3500
3000
2500
2000
1500
1000
500
0
0
40
60
80
100
120
140
Time after 3-MCA injection (days)
j
Tumor incidence (%)
100
80
60
40
20
0
0
40
60
80
100
120
140
Time after 3-MCA injection (days)

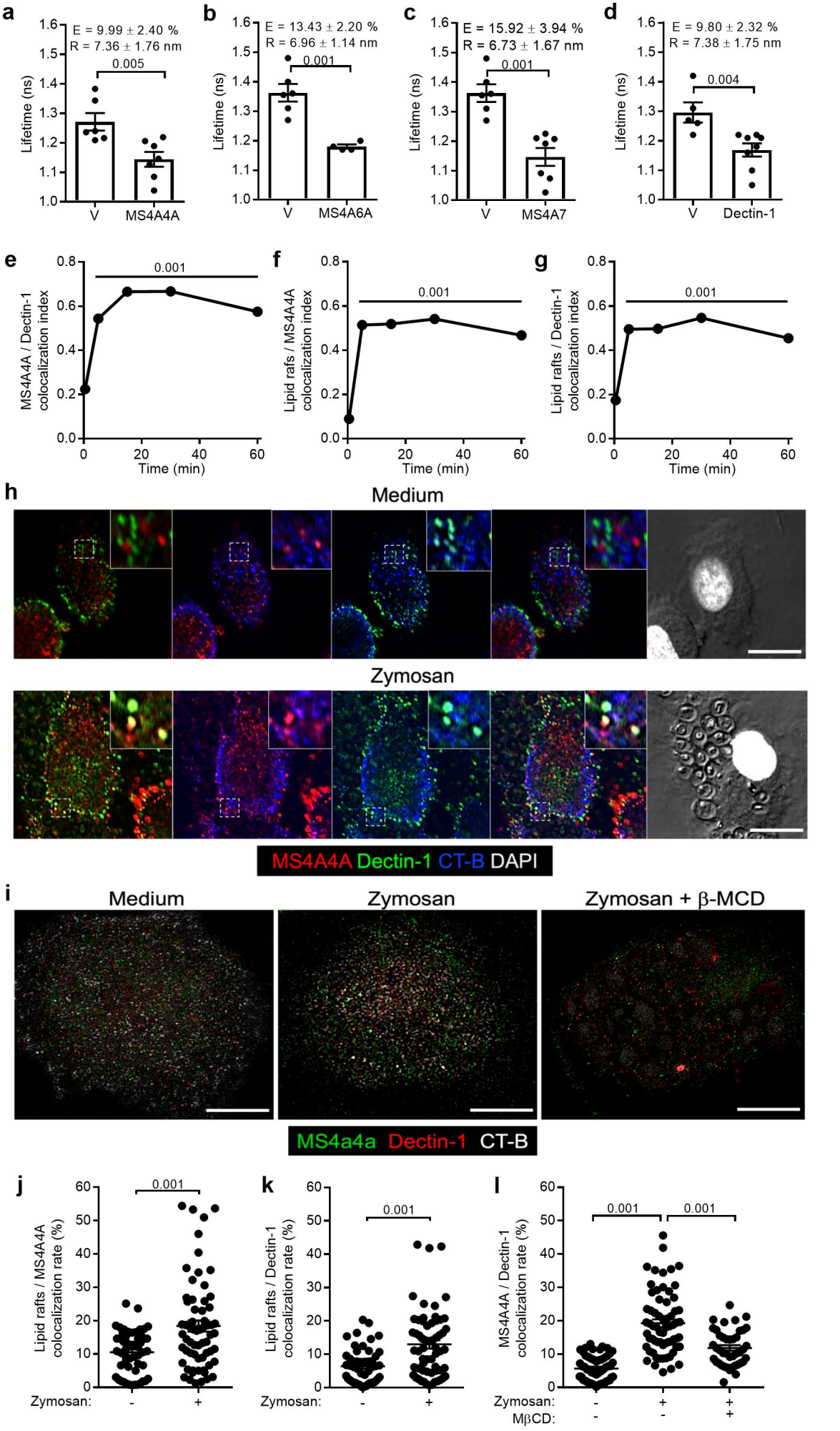
a
E = 9.99 ± 2.40 %
R = 7.36 ± 1.76 nm
0.005
Lifetime (ns)
V
MS4A4A
b
E = 13.43 ± 2.20 %
R = 6.96 ± 1.14 nm
0.001
V
MS4A6A
c
E = 15.92 ± 3.94 %
R = 6.73 ± 1.67 nm
0.001
V
MS4A7
d
E = 9.80 ± 2.32 %
R = 7.38 ± 1.75 nm
0.004
V
Dectin-1
e
MS4A4A / Dectin-1 colocalization index
0.001
Time (min)
f
Lipid rafs / MS4A4A colocalization index
0.001
Time (min)
g
Lipid rafts / Dectin-1 colocalization index
0.001
Time (min)
h
Medium
Zymosan
MS4A4A Dectin-1 CT-B DAPI
i
Medium
Zymosan
Zymosan + β-MCD
MS4a4a Dectin-1 CT-B
j
Lipid rafts / MS4A4A colocalization rate (%)
0.001
Zymosan: - +
k
Lipid rafts / Dectin-1 colocalization rate (%)
0.001
Zymosan: - +
l
MS4A4A / Dectin-1 colocalization rate (%)
0.001
0.001
Zymosan: - + +
MβCD: - - +

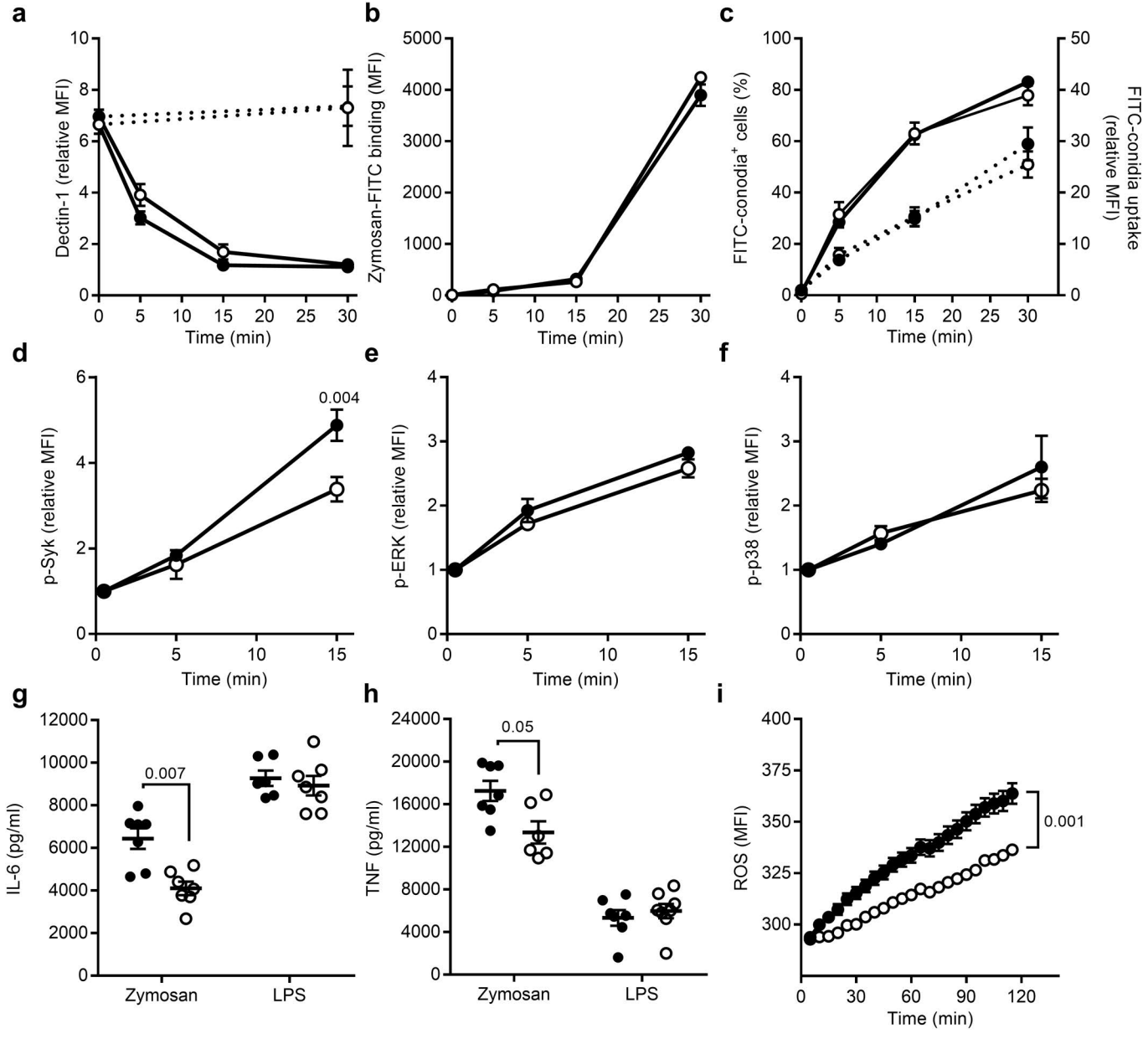
a
Dectin-1 (relative MFI)
Time (min)
b
Zymosan-FITC binding (MFI)
Time (min)
c
FITC-conodia+ cells (%)
FITC-conidia uptake (relative MFI)
Time (min)
d
p-Syk (relative MFI)
0.004
Time (min)
e
p-ERK (relative MFI)
Time (min)
f
p-p38 (relative MFI)
Time (min)
g
IL-6 (pg/ml)
0.007
Zymosan
LPS
h
TNF (pg/ml)
0.05
Zymosan
LPS
i
ROS (MFI)
0.001
Time (min)

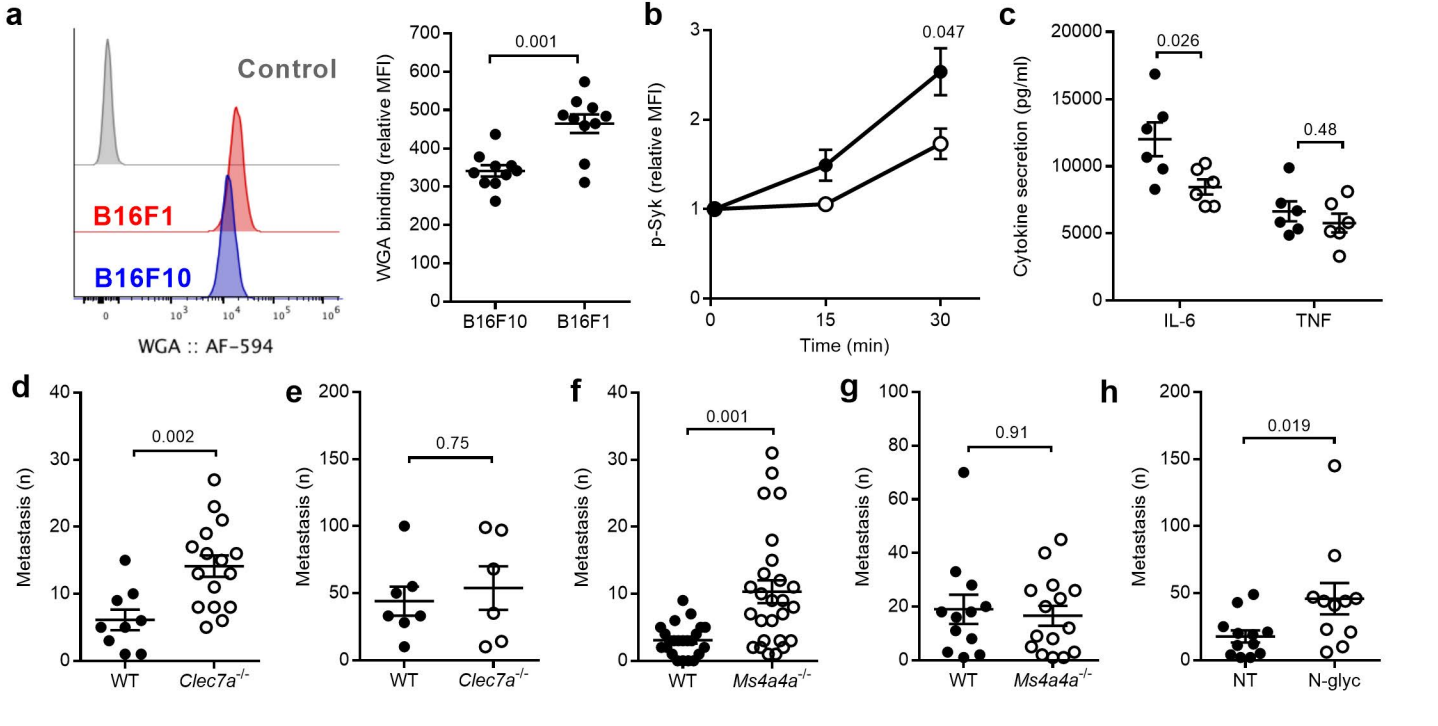
a
Control
B16F1
B16F10
WGA :: AF-594
WGA binding (relative MFI)
0.001
B16F10
B16F1
b
p-Syk (relative MFI)
0.047
Time (min)
c
Cytokine secretion (pg/ml)
0.026
0.48
IL-6
TNF
d
Metastasis (n)
0.002
WT
Clec7a-/-
e
Metastasis (n)
0.75
WT
Clec7a-/-
f
Metastasis (n)
0.001
WT
Ms4a4a-/-
g
Metastasis (n)
0.91
WT
Ms4a4a-/-
h
Metastasis (n)
0.019
NT
N-glyc

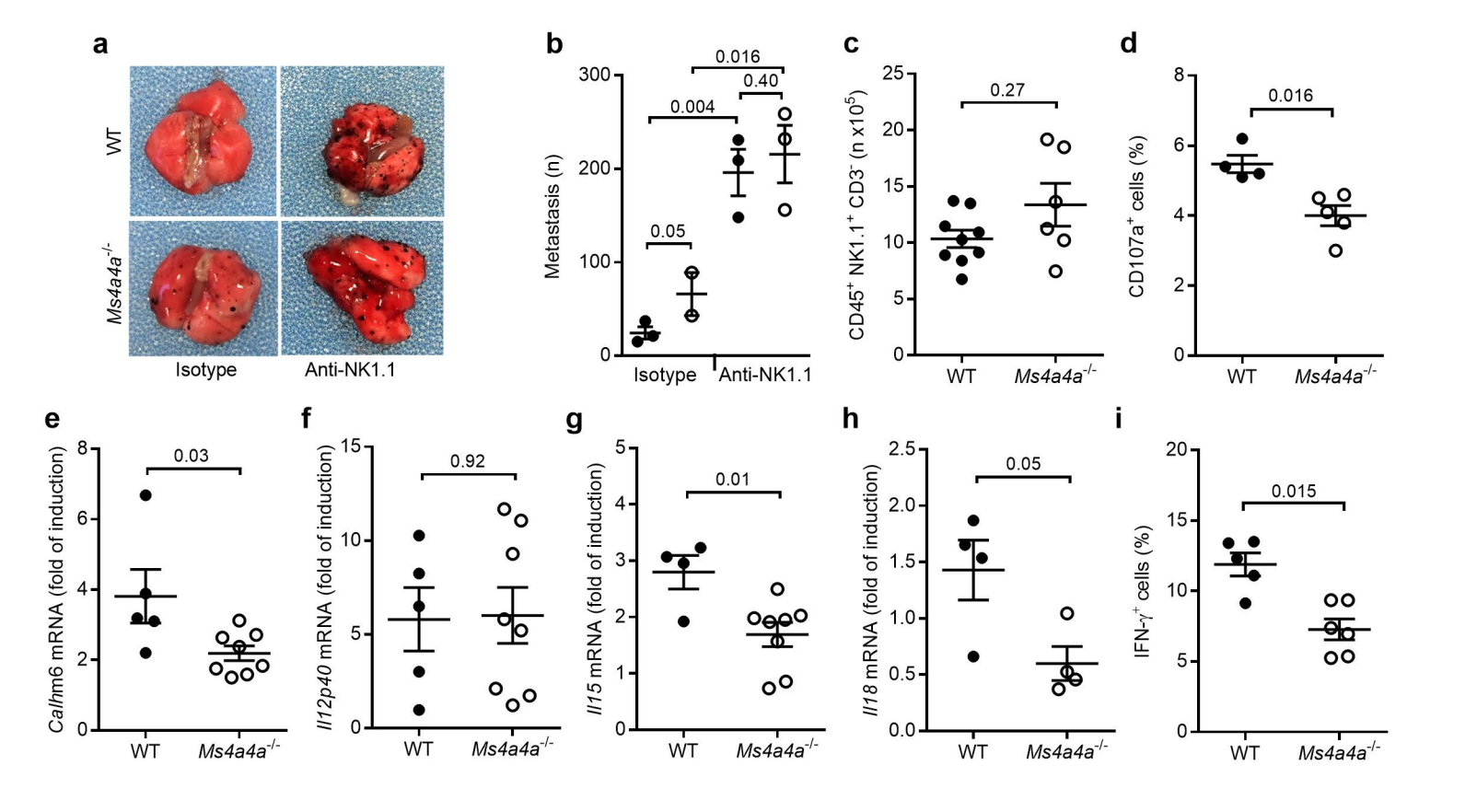
a
WT
Ms4a4a-/-
Isotype
Anti-NK1.1
b
Metastasis (n)
0.016
0.40
0.004
0.05
Isotype
Anti-NK1.1
c
CD45+ NK1.1+ CD3- (n x10^5)
0.27
WT
Ms4a4a-/-
d
CD107a+ cells (%)
0.016
WT
Ms4a4a-/-
e
Calhm6 mRNA (fold of induction)
0.03
WT
Ms4a4a-/-
f
Il12p40 mRNA (fold of induction)
0.92
WT
Ms4a4a-/-
g
Il15 mRNA (fold of induction)
0.01
WT
Ms4a4a-/-
h
Il18 mRNA (fold of induction)
0.05
WT
Ms4a4a-/-
i
IFN-γ+ cells (%)
0.015
WT
Ms4a4a-/-